AERODYNAMIC CHARACTERISTICS OF AN ELLIPTICAL CYLINDER

By

AMIT BHATNAGAR

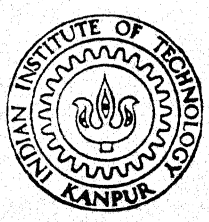

DEPARTMENT OF AEROSPACE ENGINEERING

DIAN INSTITUTE OF TECHNOLOGY KANPUR

MAY, 1991

AERODYNAMIC CHARACTERISTICS OF AN ELLIPTICAL CYLINDER

A Thesis Submitted

In Partial Fulfilment of the Requirements

for the Degree of

MASTER OF TECHNOLOGY

by

AMIT BHATNAGAR

to the

DEPARTMENT OF AEROSPACE ENGINEERING

INDIAN INSTITUTE OF TECHNOLOGY, KANPUR

MAY, 1991

CERTIFICATE

This is to certify that the thesis entitled 'Aerodynamic Charecteristics of an Elliptical Cylinder ', is a record of the work carried out under my supervision by Mr. Amit Bhatnagar and that it has not been submitted elsewhere for awarding a degree.

A. K. Gupta

Dated:

(Dr. A. K. Gupta)
Professor & Head
Dept. of Aerospace Engg.
I.I.T. Kanpur -208 016

ACKNOWLEDGEMENTS

I am immensely grateful to Dr. A. K. Gupta for his perseverance, guidance, patience and encouragement at every stage of the thesis.

The study owes a great deal to Dr. M. Krishnamurthy, Assistant Director NAL, who has assisted the study by kindly providing the model, the literature and his valuable guidance.

I am also beholden to Shri K. S. Muddappa for his assistance and the willingness with which it was offered.

I am indebted to my senior, Mr. B. K. Anand for helping me with the dynamic signal analyser and making available his time, whenever required.

I am very proud of my friendship with Mr. Rajeeva Kumar, whose assistance stretches from typing the manuscript to active criticism and pertinent suggestions.

Thanks are also due to my friends Abhai, Manoj, Navdeep for performing numerous small tasks that go into the making of a thesis.

ABSTRACT

The objective of this study is the enhancement of existing experimental data on the aerodynamic characteristics of cylinders of elliptical cross section. The model used in the study has the fineness ratio of 1.5. Tests were conducted at different angles of attack ranging from zero degree to ninety degree in steps of ten degree and at three different Reynold Numbers in subsonic zone. The model was mounted horizontally in the 2-D wind tunnel. The pressure distribution over the surface was determined with the help of a water multitube manometer and was used to calculate the lift, drag and moment coefficients for various angles of attack. The vortex shedding frequency was determind by a hot wire anemometer linked to dynamic signal analyser based on FFT technique.

The variation of drag coefficient, lift coefficient and moment coefficient of the model, with angle of attack is presented for three different wind speeds. Free stream turbulence level is also determined for the operating range of speed. Similarly Strouhal no is plotted against the angle of attack for diffrent wind speeds. The calculated values of Strouhal nos. compare reasonably well with the reported data in the literature.

CONTENTS

LIST OF SYMBOLS

C_D = Drag coefficient (page 19, 25)

C_L = Lift coefficient (page 21, 25)

C_M = Moment coefficient (page 22, 26)

C_p = Pressure coefficient (page 18, 31)

D = Drag force (page 19)

i = Number of tap point, measured in the anti clockwise direction, with the tap point at the leading edge being one, as shown in figure A.1 (page 15, 19, 21, 22)

L = Lift force (page 21)

M = Total moment acting on the body, about the centre taken positive in the clockwise direction (page 22)

Q = Dynamic pressure head of freestream (page 18, 19, 21, 22)

P_i = Pressure at angular distance (θ) measured from the leading edge in the anti clockwise direction (page 18)

P_0 = Stagnation pressure of freestream (page 18)

P_s = Static pressure of freestream (page18)

Re = Reynolds No. (page 22)

St. No. = Strouhal number (page 22)

LIST OF FIGURES

CHAPTER 1

INTRODUCTION

1.1 INTRODUCTION TO ELLIPTIC CROSS SECTION

In recent years, elliptic cross sections have acquired a great deal of significance, especially in the context of missile configurations and aircraft noses. These cross sections offer considerable aerodynamic advantages over the conventional circular ones, especially at high angles of attack. The actual cross section is not exactly elliptical as the upper surface is more convex than the lower half. However, since elliptical cross sections are the simplest geometrical shapes to approximate them, the present work has been done on elliptical cross section

. The data existing in the published literature on enquiry turned out to be meagre. While the country has embarked on an ambitious missile (I.G.M.D.P.) and aircraft (L.C.A. & L.T.A.) developement programmes, the importance of such experimental data can hardly be underestimated.

Allen, H. Jullian and Perkins, Edward W.[1] (1951) have given a method for estimating the effects of viscosity on the forces and moments for inclined bodies. In their recommended method, they have tried to correlate the cross flow in planes perpendicular to the inclined axis of the body to the flow around a cylinder and hence, the resulting cross forces are related to the section drag coefficient. The use of this method requires a knowledge of the section drag characteristics of the cylinder at different angles of attack. In the era of terrain mapping missiles, whose trajectory changes continously in response to topological changes, the angle of attack of cross flow will also vary continously, leading to a change in forces and moment acting on the missile. Since drag coefficient is different at different angles of attack, the mean pressure distribution will also be different. Similarly the vortex shedding frequency is a function of angle of attack and hence the fluctuating pressure acting on the cylinder will also vary as angle of attack changes in response to changes in trajectory.

The motivation for the study came with the successes notched up by the country's space scientists in successfully firing missiles after missiles of

diverse capabilities. A second motivating factor was the highly sophisticated dynamic signal analyser recently acquired by the aerodynamics laboratory at considerable expense and which can be employed to measure the shedding frequency in turbulent wakes.

1.2 LITERATURE REVIEW

Extensive research into literature reveals that very little data exists on cylinders of elliptical cross section. The field has attracted a few researchers but most of their work is of a perfunctionary nature and fails to cover the subject exhaustively.

Noel K. Delany and Norman E. Sorenson[2](1953) have conducted detailed experiments to study the approximate variation of drag coefficient with Reynolds Number of several cylinders having different cross sectional shapes. They obtained data for cylinders having cross sectional shapes of circle , ellipse of two fineness ratios (1:2 and 2:1), rectangle, diamond and two isosceles triangles. Data was obtained for Reynolds Number as low as 11000 and as high as 2.3×10^6. The vortex shedding frequencies were measured and drag coefficients were determined.

For the ellipse, they plotted a graph showing the variation of the drag coefficient and Strouhal Number vs Reynolds number. For Reynolds Number less than 10^5 the Stouhal frequency was approximatly 0.2 . This value provides a confirmation for the results of the present experimental study.

V. J. Modi and E. Wiland[6] (1970) have experimentally studied the aerodynamics of a set of two dimensional elliptical cylinders with eccentricity of 0.8 and 0.6, during organised wake conditions. The data on Strouhal Number, unsteady pressures and wake geometry is presented as a function of angle of attack during static condition of the model. The effect of Reynolds Number on the fluctuating pressure is also examined. The results indicate dependence of the unsteady forces on Reynolds Number at zero angle of attack. The model has thirty pressure tap points distributed all along the surface. They have given graphs showing the variation of Strouhal Number with angle of attack. They have also plotted the variation of mean pressure coefficients over its surface for four different angles of attack ($\alpha = 0^0, 30^0, 60^0, 90^0$).

1.3 Scope of the Present Study

In the present study the objective is to measure the presssure distribution over an elliptic cylinder and to determine the lift coefficient, the drag coefficient, the moment coefficient at various wind speeds and varying angles of attack. The experiment was repeated to measure the Strouhal frequency again at different angles of attack and different wind speeds

CHAPTER 2

EXPERIMENTAL EQUIPMENT

2.1 WIND TUNNEL

The subsonic wind tunnel (known as 5 - D tunnel) at aerodynamics laboratory was used. It is a close circuit type having a rectangular cross section of 1'x4' with a length of 5'6". The characteristics of the motor are as follows :

	SCR	DC	Blower Drive	
	Twin		15 HP	
Input	400V.	50 cycles	3ϕ	
	57 - 98 - 57 amperes			
output	Armature	115V	110 ampere	DC
	Field	115V	5-7 ampere	DC

The motors are turned on by pressing the start buttons of respective units and their speeds are then controlled by manual speed adjusting potentiometers. The maximum velocity obtainable is 42m/s. The wind tunnel has a plexiglass window with a circular groove in which a disk can rotate. The opposite side has a wooden trapdoor concentric with the circular groove in the plexiglass.

2.2 Pitot Static Tube

For measuring the wind speed a pitot static tube was used. The pitot static tube was placed far upstream in the flow and the pressure measurements were taken by the water manometer inclined at 30^{0} with the vertical.

2.3 FC012 Micromanometer

The pitot static tube was connected to a FC012 micromanometer. It is supplied by Furness Ltd. It can measure water height upto 19.9 mm and wind speed upto 64 m/s. The values can be directly read off the digital display.

2.4 Water Manometer

It is an ideal instrument for pressure measurement. Inspite of its simplicity it can measure pressures with great accuracy. The multitube inclined water manometer was used. The tubes are inclined at 30° to the vertical to increase the sensitivity.

2.5 Hot Wire Anemometer :

It has been used to measure the frequency of vortex shedding by the elliptic cylinder. It uses a Hot-wire as a transducer and is designed to measure the instantaneous mass flow of gasses and liquid. It is ideal for measuring high frequency flow fluctuations. It is based on the principle of convective heat loss in an electrically heated wire by the flow of gas or liquid surrounding the wire. It basically determines the amount of power required to keep the temperature constant. The anemometer used is DISA 55A01 constant temperature type. The hot wire is 10 % Rhodium and 90 % platinum. It has a resistance of 40 Ω/cm at 20° C. The length of the platinum wire is 1mm and diameter, 0.00762 mm . So the l/d ratio becomes 132.23 which is greater than 100 as required.

2.6 Oscilloscope :

It can measure frequency response upto 0 – 60 kc/s The signal from hot wire has been monitored continously on a DSS 50 20A portable dual channel digital storage oscilloscope. It is incorporated with an 8 – bit CPU, with a maximum sampling rate of 1 MHz and effective storage frequency of 40 db Hz and a memory capacity of 1024 words per channel. The saved waveforms can be displayed being magnified upto 100 times .

2.7 Dynamic Signal Analyser :

This is a powerful instrument to analyse the incoming signals either in the frequency domain or time domain. It works on the basis of FFT(Fast Fourier Transform). Such an analyser is useful for the analysis of the signals in the range of a few millihertz to about a hundred kilohertz. An important property of FFT is that if the time record has N equally spaced samples then the FFT transformation from time domain to frequency domain contains only N/2 equally spaced lines. This is because in the frequency domain, each line actually contains both amplitude and phase. The samples can be averaged over a short time or long time. The obtained spectra can be stored in a floppy for later use or can be directly fed into a computer or a plotter. Sensitive to small signals, it is operable in a dry environment upto 40° C. In the present investigation a HP spectrum analyser is used. It can perform a few mathematical operations like FFT, inverse FFT, conjugate, separation into real and imaginary parts etc. Further, one can define one's own mathematical functions which make use of either the present data or some stored data.

CHAPTER 3

EXPERIMENTAL TECHNIQUE AND MODEL MOUNTING

3.1 MODEL

The model was made of fiber reinforced plastic by means of casting. Initially a wooden model of elliptic cylinder was made. The major axis was kept at 10.5 cm and minor axis at 7.0 cm. The length of the cylinder is 31 cm. With the help of the wooden model, the mould was made. This mould was used for making the FRP model. A core was used for making a through hole in the model. The model was then painted in order to get a smooth surface and reduce skin friction. In order to measure the pressure, pressure tap points were required. Holes were made on the surface of the model by means of counterboring machine. The holes were made in a plane which was equidistant from either of the end surfaces. The holes were made approximately at angular distances of 10^0 . At the leading edge , holes were made at angular distances of 5^0 in order to get higher accuracy. In all 44 pressure tap points were made. The position of the pressure tap points is given in fig A.1 and table A.2(Appendix A) . The pressure tap point at the leading edge is numbered one and after that the points are numbered sequentially in an anticlockwise direction. Small metallic tubes of bore 1mm were bent at 90^0 and inserted into the holes after heating. These metallitic tubes were inserted into the tap points after pushing them through the central hole in the model. These metallic tubes were then attached by means of rubber tubing to the manometer. All these rubber tubing were taken out through the central hole of the model. The model was fabricated at the Experimental Aerodynamics Division Laboratory, NAL Banglore and was kindly provided by Dr. M. Krishnamurthy, Astt. Director, EAD, NAL Banglore.

3.2 MOUNTING OF THE MODEL

The model was mounted on the wind tunnel with its axis horizontal and perpendicular to the flow. Two flat discs were attached to the model at either end. The discs were screwed into the model so that they can be removed, when required. One disc was made of wood and fitted into a corresponding blind hole made into the wooden trapdoor of the wind tunnel. The other disc was made of plexiglass and was made to fit the circular groove in the plexiglass window. This

disc has a hole through which the rubber tubings connected to the manometer can be taken out. Both the discs were made freely rotating in their grooves. A wooden T was made to fit the hole in the plexiglass disc and was used for rotating the elliptic cylinder. Thereby the angle of attack could be changed.

In order to determine the 0^0 angle of attack, the wind tunnel was started at any speed. At zero degree angle of attack the stagnation pressure of pitot static tube and the pressure at the leading edge of the model should be exactly same. The position was determined by rotating the model and checking the pressures till they are equal. A marker was attached to the plexiglass disc to correspond to zero degree and markings were made on the circular groove at angular distances of 10^0.

3.3 EXPERIMENTAL TECHNIQUE

Initially, the turbulence level in the wind tunnel was determined by means of a hot wire probe. The hot wire probe was connected to DISA type 55D26 signal conditioner & DISA type 55M10 CTA standard bridge from which the signal was taken to a DISA type 55D31 digital voltmeter and a DISA type 55D35 RMS unit. The pitot static tube was connected to FC012 Furness micromanometer, which directly gives the wind speed in the tunnel. The initial mean value of the voltage of Hot Wire at zero wind was read. The temperature, cold resistance and the operative resistance were also read. Then the wind tunnel was started and the potentiometer was adjusted so that the speed in the wind tunnel is in the same zone as the one in which experiments are to be conducted. At a fixed speed the mean and rms values of voltage of Hot Wire are read. Then the wind speed is changed and the process gets repeated.

The model was mounted and the pressure taps were connected to the water manometer. The heights of the water columns in all the 44 tubes of manometer were read. Then the wind tunnel was started and the heights of water columns in all the 44 tubes of the manometer were recorded. The heights of the water columns in the U - tubes connected to a pitot static tube were also recorded. Then the angle of attack was changed by 10^0 and the whole process was repeated. It was done till the angle of attack became 90^0. Then the wind speed was changed and the whole set of data was again collected. This was done for three different wind speed.

For measuring the vortex shedding frequency hot wire anemometer was

used It was connected to dynamic signal analyser and an oscilloscope The hot wire probe was placed at a distance of 6a (a = semi-major axis of the elliptic body) downstream from the cylinder A vortex detector was used to find the exact position of the Karman vortex street, so that the hot wire probe can be located there. After locating the probe in the vortex street, voltage fluctuation was studied on the oscilloscope. If the probe is located correctly the voltage fluctuates wildly. The dynamic signal analyser is programed to take 15 sets of data. The vortex shedding frequency was also determined at three different speeds and different angles of attack (in steps of 10)

CHAPTER 4

RESULTS AND DISCUSSION

4.1 Data Reduction

4.1.a Turbulence Level

The turbulence level in the wind tunnel for different wind speeds was determined by means of the following formula

$$\text{Turbulence intensity} = \frac{e_{rms}}{1000} \times \frac{4\,E}{E^2 - E_0^2}$$

where

e_{rms} = rms value of voltage in millivolt

E = mean value of Hot Wire voltage at a given wind tunnel setting.

E_0 = mean value of Hot Wire voltage at zero wind.

4.1b Pressure Coefficient

The pressure at each tap point for each wind tunnel run and angle of attack setting, is measured by means of the following formula (as the height of the water column in the manometer is read in cm, all calculations are shown in C.G.S. units for greater accuracy and simple calculations)

$$P_i = \rho\, g\, h_i \sin\beta$$

where

P_i = pressure at the ith tap point in dynes

ρ = density of water in gm/cc

g = acceleration due to gravity in cm/sec^2

h_i = (initial height of ith water column

— present height of ith water column)

β_i = angle which the water column tubes make with the horizontal.

The dynamic pressure head (Q) is measured by the following formula

$$Q = \rho g h_{ps} \sin\beta$$

= dynamic pressure in dynes/cm^2

h_{ps} = difference between the heights of water column in the two arms of U - tube connected to pitot static tube

The stagnation pressure is the same as the pressure at the leading edge of the model when it is inclined to the wind direction at 0° angle of attack.

The static pressure is determined by the following formula

$$P_s = P_0 - Q$$

where

P_s = static pressure of wind in dynes/cm^2

P_0 = stagnation pressure of wind in dynes/cm^2

The stagnation pressure was taken to be same as the pressure at the leading edge at 0° angle of attack. The static pressure is determined by subtracting the dynamic pressure from the stagnation pressure . Since the wind velocity was kept constant at all angles of attack the stagnation pressure was assumed to be constant at all angles of attack.

The pressure coefficient at each pressure tap point is determined by the following formula

$$C_{P_i} = \frac{P_i - P_s}{Q}$$

where

C_{P_i} = pressure coefficient at ith tap point

4.1c Drag Coefficient

The total drag force was determined by calculating the total force acting on the model along the direction of the wind speed.

Let the major axis of the cross section correspond to X axis, positive direction being towards the trailing edge and the minor axis correspond to Y axis, positive direction being counter clockwise to x-axis. The equation of the ellipse is

determined by the following formula

$$\frac{x_i^2}{a^2} + \frac{y_i^2}{b^2} = 1$$

where

x_i = x co-ordinate of ith tap point

y_i = y co-ordinate of ith tap point

a = semi-major axis of the ellipse

b = semi-minor axis of the ellipse

The slope of the tangent to the ellipse at the ith pressure tap point is

$$m_1 = -\frac{b}{a\, m_i}$$

The slope of the normal at ith pressure tap point is given by

$$m_2 = \frac{a}{b}\, m_1$$

where a/b is the fineness ratio.

For this study the fineness ratio was kept at 1.5. so the above relation reduces to

$$m_2 = 1.5\, m_i$$

$$\theta_i = \tan^{-1}(1.5\, m_i)$$

where θ_i is the angle between the normal and the x-axis.

The pressure P_i at each pressure tap point acts along the normal at that point.

Now to determine the force, a small element of the perimeter is taken. The force element acting at ith tap point is given by

$$df = P_i\, r_i\, \Delta\theta_i'$$

This force element acts on a surface element of unit length and width $r\Delta\theta_i'$

where

r_i = the distance of ith tap point from the centre of ellipse

$$= (a^2 \cos^2\theta_i' + b^2 \sin^2\theta_i')^{1/2}$$

θ_i' = the angular distance of line joining ith tap point from the +ve x axis, measured +ve in counter clockwise direction.

$$\Delta\theta_i' = \frac{\theta'_{i+1} - \theta'_{i-1}}{2}$$

Let α be the angle of attack. Then, the angular distance (θ) between the direction in which the force element acts and the wind speed direction is

$$\theta = \theta_i - \alpha$$

Now this force element can be resolved into two components, along the wind speed direction and perpendicular to it.

The component of the force element acting at ith point along the wind speed direction is $df_i \cos(\theta_i - \alpha)$
so drag force is given

$$D = \sum_{i=1}^{44} -(P_i\, r_i\, \Delta\theta_i')\cos(\theta_i - \alpha)$$

and the drag coefficient is

$$C_D = \frac{D}{Q\ 2a}$$

4.1d Lift Coefficient

The component of the force element acting at ith point perpendicular to the wind speed direction is $df_i \sin(\theta_i - \alpha)$
so lift force is given by

$$L = \sum_{i=1}^{44} -(P_i\, r_i\, \Delta\theta_i')\sin(\theta_i - \alpha)$$

and the lift coefficient is

$$C_L = \frac{L}{Q\ 2a}$$

4.1e Moment Coefficient

The moment about the center of the ellipse acting on the cylinder due to the force element df_i acting at point 'i' is given by

$$d\vec{m}_i = \vec{r}_i \times d\vec{f}_i$$
$$= a\ df_i \sin\theta_i\ \cos\theta_i' - b\ df_i \cos\theta_i\ \sin\theta_i'$$

so the total moment acting on the cylinder

$$M = \sum_{i=1}^{44} (P_i\ r_i\ \Delta\theta_i')\ (a \sin\theta_i\ \cos\theta_i' - b\cos\theta_i \sin\theta_i') \quad \text{in dyne-cm}$$

The moment is taken as +ve if acting in clockwise direction. The moment coefficient is given by

$$C_M = \frac{M}{Q\ (2a)\ (2b)}$$

4.1f Strouhal Number

The Strouhal number is given by $= \frac{f\ d}{U_\infty}$

where

f = frequency of vortex shedding by the cylinder in Hz.

d = 2 b in meter

U_∞ = free stream velocity in m/sec

Here for 'd', the minor axis has been taken in order to compare the results with the values obtained by Delany[2]

4.1g Reynold No.

$$\text{Re No.} = \frac{\rho_a\ U_\infty\ d}{\mu}$$

where

ρ_a = density of air in kg/m^3(1.225 kg / m^3)

U_∞ = free stream velocity in m/sec.

d = 2 a in meter

μ = kinematic viscosity kg /m - sec(0.000014607 kg /m - sec)

4.2 Results.

4.2a Turbulence Level

The turbulence level in the operating zone turned out to be considerably high. The values are given in table a.1. It is more than 1.8% for all the three wind speeds, whereas ideally it should be less than 0.5%. Since free stream turbulence is high, it will make the boundary layer unstable and induce transition from laminar to turbulent boundary layer much earlier than normal circumstances.

4.2b Pressure Coefficient

The distribution of pressure coefficients over the surface of cylinder for different angles of attack is plotted from fig. b.1 to b.10 . The three curves show the distribution of pressure coefficient for different Reynolds no. If we study fig b.1, all the three curves appear to be quite symmetrically distributed about an axis passing through x = 180°. This means that the distribution of pressure coefficients over the top surface of the cylinder is quite similar to the distribution of pressure coefficients over the bottom surface of the cylinder. Since the pressure distribution is quite identical over both the surfaces, the total lift force is nearly zero. The pressure coefficient remains constant from 120° to 240°. This means that the flow separation has taken place. Therefore the flow separates at about 120° from the leading edge for both the upper edge and the lower edge. The graph is quite similar to that obtained by Modi[3] in its general pattern. The C_p has a maximum value at θ = 0°. In the case of Modi's graph (fig 6.a)[3] the pressure in the wake region is almost constant whereas in the present case it fluctuates slightly.

If we study fig b.2 we find that a large suction pressure develops over the upper surface, between 0° to 100° whereas on the bottom surface the pressure remains positive only upto 40° and then becomes negative. However the value of the suction pressure on the bottom surface is very small. Therefore a very large lift force is generated. The pressure remains nearly constant from 120° to 240°.

Therefore the flow separation takes place at 120° on the bottom surface and 60° on the upper surface.

Next we consider fig b.3. It is quite similar to fig b.2. There is a very large value of suction pressure on the top surface and small value of suction pressure on the bottom surface. However if we compare it with fig b.2, we find that the suction pressure acting on the upper surface in fig b.3 is more than that in fig b.2 and therefore a larger lift force is generated at angle of attack of 20°. The flow separates at about 120° on the bottom surface and 130° on the upper surface.

Next is fig b.4. Here for Reynolds no. 2.29 x 10^5 and 2.59 x 10^5 , the suction pressure on the upper and the bottom surfaces are nearly equal and therefore they cancel out each other. There is a very small value of positive pressure acting on bottom surface between 0° to 60° which is responsible for generating some lift. However the lift is substantially lower than in fig b.2 and fig b.3. The flow separates at about 120° on the bottom surface and about 30° on the upper surface. These curves represent typical stall characteristics. However the curve for Re. no. 3.06 x 10^5 differs and developes a large suction pressure on the top surface. This results in a large lift force. This behavior is difficult to explain theoretically. This may be due to experimental error. The graph on comparision with Modi's (fig 6.b)[3] turns out to be quite similar.

Fig b.5 corresponds to α = 40°. Here again flow separates on the upper surface at about 20° whereas on the bottom surface it separates at about 140°, a small value of positive pressure acting on the bottom surface generates a small lift.

Fig b.6 to fig b.10 are quite similar. In all the cases the flow separates quite early on the upper surface and very late on the bottom surface. For fig b.6, the flow separates at 140° on the bottom surface and 10° on the upper surface. For fig b.7 to fig b.10 the values are 160° on the bottom surface and 10° on the upper surface. The fig b.7 & fig b.10 show good resemblance to Modi's graphs (fig 6.c & fig 6.d respectively)[3].

In all these curve, we also see that the maximum value of C_p occurs at the tap point coresponding to the angle of attack. This is where the wind loses it entire kinetic energy and C_p attains it maximum value.

4.2c Lift Coefficient vs α

Fig b.11 shows the variation of the lift coefficient vs angle of attack for the three Re. Nos. The three curves match perfectly but for one value at 30° for Re. no. of 3.06×10^5 . This anomaly becomes clear by viewing fig b.4 where, as observed, a large suction pressure develops over the top surface resulting in a large lift force. This may be due to experimental error.

The lift coefficient is nearly zero for zero degree angle of attack. Ideally speaking, it should be exactly zero. But because of the practical difficulty of locating the exact position of the 0° angle of attack it ends up having small value.

The lift coefficient increases rapidly for the next angle of attack and continues to rise upto α = 20°. After that the lift coefficient drops suddenly representing typical stall characteristics . Thereafter the lift coefficient remains more or less constant ,rising slightly to attain a local maximum at α = 50°. It finally becomes zero for α = 90° . The curve for Re. no. 3.06 x 10 differs slightly by having a large value of C_L for α = 30° .This is due to large suction pressure on the upper surface as evidenced by fig. b.4.

4.2d Drag Coefficient vs α

The graph in fig b.12 shows the variation . The drag coefficient is slightly high for α = 0°.This is because of flow separation as visible in fig b.1. After this the drag coefficient drops and continues to have a small value for the next angle of attack too .These two points refer to the zone where large lift force is generated .After that it rises rapidly till α = 70°. After this point it rises more gradually and finally attains its maximum value at α = 90°. The drag coefficients for zero angle of attack at all Re. nos. are approximately 0.4, whereas in the case of Delany[2] they are more than 0.6. Delany[2] has not given free stream turbulence level at which the experiment was conducted. The high turbulence level in the present study might be responsible for early transition from laminar to turbulent boundary layer, hence low value of drag coefficient.

4.2e Moment Coefficient vs α

The relationship is plotted in fig b.13 The moment coefficient is zero at zero degree of angle of attack because of symmetricity of pressure distribution over the two surfaces. As the angle of attack is increased ,the moment coefficient increases for α = 10° and reaches its peak value at α = 20° .After that it drops rapidly till 40° .After that it remains nearly constant , attaining a local maximum at α = 60° It also drops to zero for 90° of angle of attack

4.2f Strouhal Number vs α.

The spectral records for 0° and 10° angle of attack for Re. no. 2.75×10^5 and 3.18×10^5 do not give a clear peak. The curve remains more or less constant over a large range . The slight fluctuations might be due to voltage fluctuations and it is very difficult to determine the peak. The three spectral records are put at the end of Appendix C, the first one corresponding to Re. no. 2.75×10^5 and α = 0° .The last two similarly for Re. no. 3.18×10^5 and α = 0° and α = 10°. The variation of the St. number vs angle of attack is plotted in fig.b.14 .The value of Strouhal number has its maximum value at 0° of angle of attack and after that it more or less continues to fall and gives its lowest value at 90°. The results obtained more or less agree with the results obtained by Modi[3]. The Strouhal no. continue to fall as the angle of attack increases. However, the Re. no. dependence is not as marked as in the case of Modi[3]. The Strouhal no. for zero degree angle of attack is approximately 0.2 as obtained by Delany[2].

CHAPTER 5

5.1 Conclusions

The pressure coefficient curves match quite well for all the Re. numbers. The pressure coefficient shows Re. no. independence. The pressure coefficient distribution over the surface is as expected. The graph for C_p vs θ for the angles of attack 0°, 30°, 60° and 90° agree very well with the results obtained by Modi[3]. Modi's[3] graphs provide confirmation for the correctness of method and allow us to conclude that the results obtained for other angles of attack are also reasonably correct. The flow serapation takes place at all the Re. numbers.

From the lift coefficient and drag coefficient curves we see that the cylinder is subjected to maximum lift force and minimum drag force when the angle of attack is 20°. The ideal angle of attack for generating large lift forces is between 10° to 20°. This fact is also confirmed by the moment coefficient curve. The maximum clockwise moment acting on the cylinder takes place at 20°. After this angle the cylinder exhibits typical stall characteristics. The lift, drag and moment coefficients show Re. no. independence.

The dynamic signal analyser turned out to be a very useful instrument as it gives the frequency of vortex shedding directly without the botheration of counting number of peaks in the trace of the storage oscilloscope. Moreover, it averages the values over 15 reading, thereby increasing the accuracy. The Strouhal no. decreases as angle of attack increases.

5.2 Scope for further work

One may study the variation of drag coefficient with Reynolds no. by collecting the data for large values of Reynolds Number and can study the effect of tripping the boundary layer on the drag coefficient. For this one may paste a small strip of sandpaper near the leading edge of the model.

One may also study the variation of the drag coefficient with changes in Strouhal number.

The pressure drag coefficient is determined from the surface pressure data and the total drag coefficient is determined from wake measurement using a rake. This can be used to determine the skin friction drag coefficient of the model.

However for this a very long wind tunnel will be necessary as in subsonic flow regime the downstream disturbances effect the flow upstream. The one available presently in the aerodynamics lab is inadequate for this job.

From the surface pressure data one can determine the separation and reattachment points. This information can be confirmed by surface flow visualization using oil flow.

In a nutshell, the field of elliptic cylinders is wide open to any student of experimental aerodynamics.

REFERENCES

1 Allen, H. Julian, and Perkins, Edward W. : "A Study of Effects of Viscosity on Flow Over Slender Inclined Bodies of Revolution". NACA Rep. 1048, 1951.

2. Delany, Noel K. & Sorenson, N. E. : " Low Speed Drag of Cylinders of Various Shapes". NACA TN 3038, Nov. 1953.

3. Modi, V. J. & Wiland, E. : "Unsteady Aerodynamics of Stationary Elliptic Cylinders in Subcritical Flow". AIAA Journal Vol 8, Oct 1970, pp 1814 - 1821.

4. Pankhurst, R C. & Holder, D. W. : " Wind Tunnel Technique", Sir Isaac Pitman & Sons Ltd., London 1968.

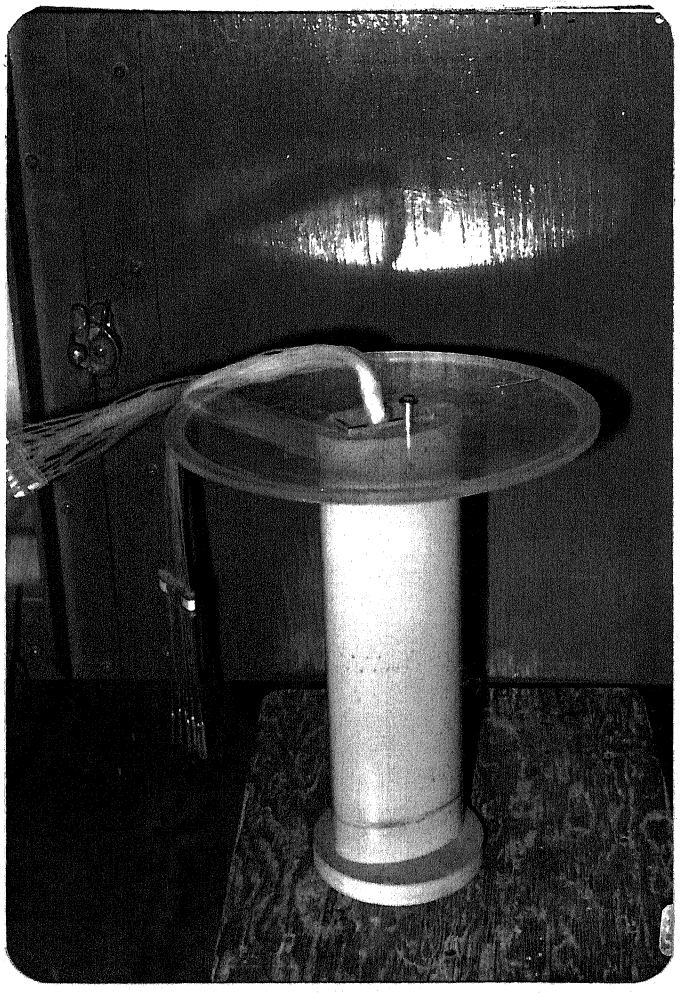

1. Model

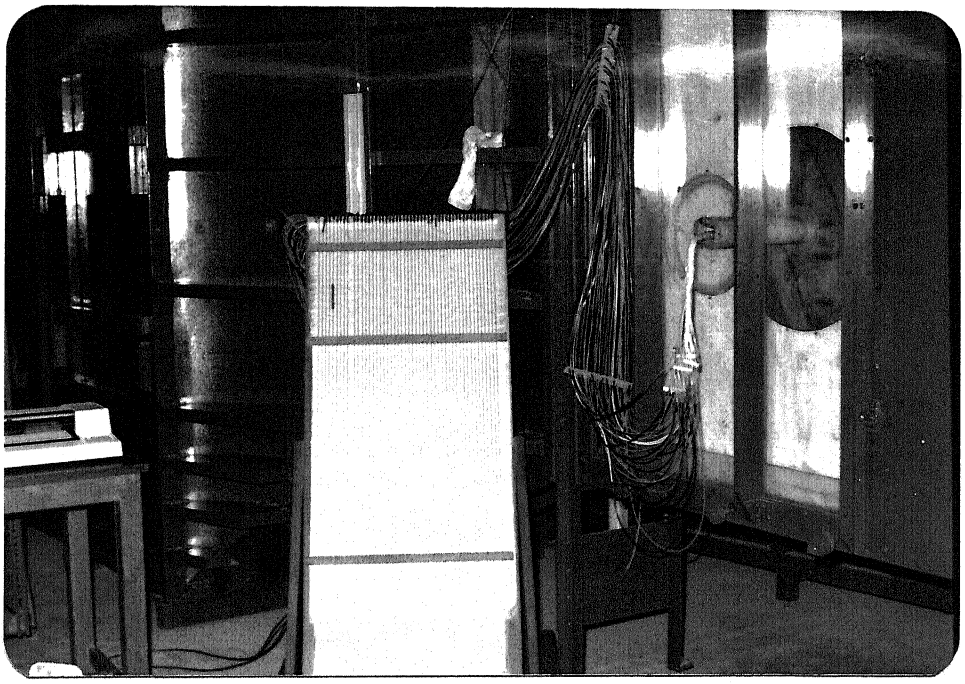

2. Model connected to water manometer

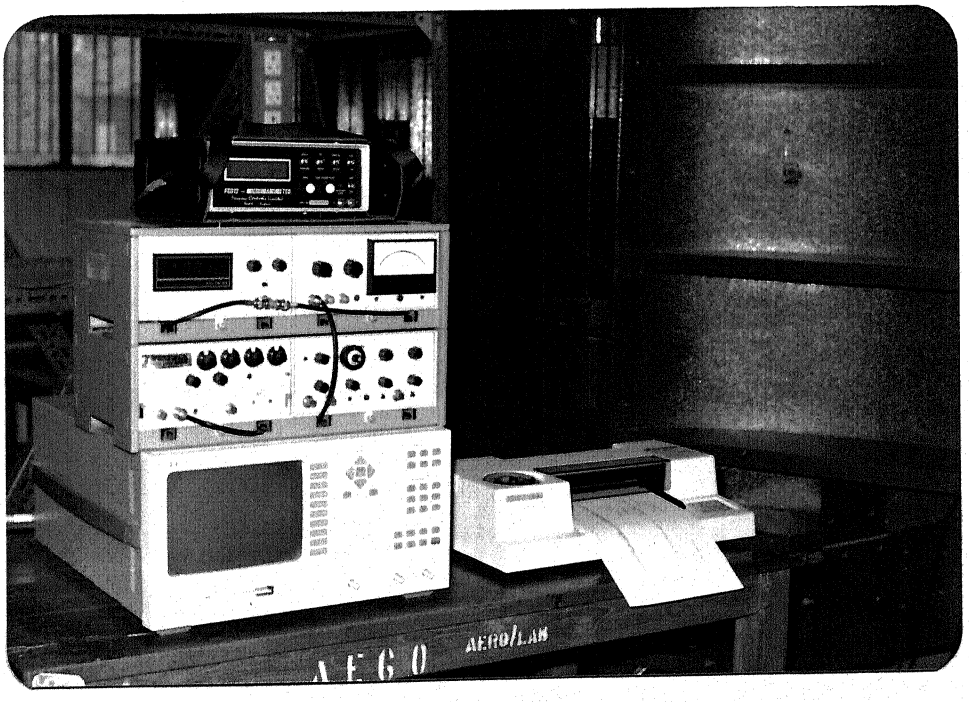

3. Model connected to Furness micromanometer, dynamic signal analyser and plotter

TABLE a.1

Temperature 301 K

Cold Resistance 3.52 Ohms

Operative Resistance 5.4 Ohms

Wind speed (m/s)	E(V)	Erms(mV)	Turbulence Intensity
28.5	6.97	18.3	1.87 %
32.5	7.09	19.2	1.88 %
38.4	7.24	19.5	1.82 %

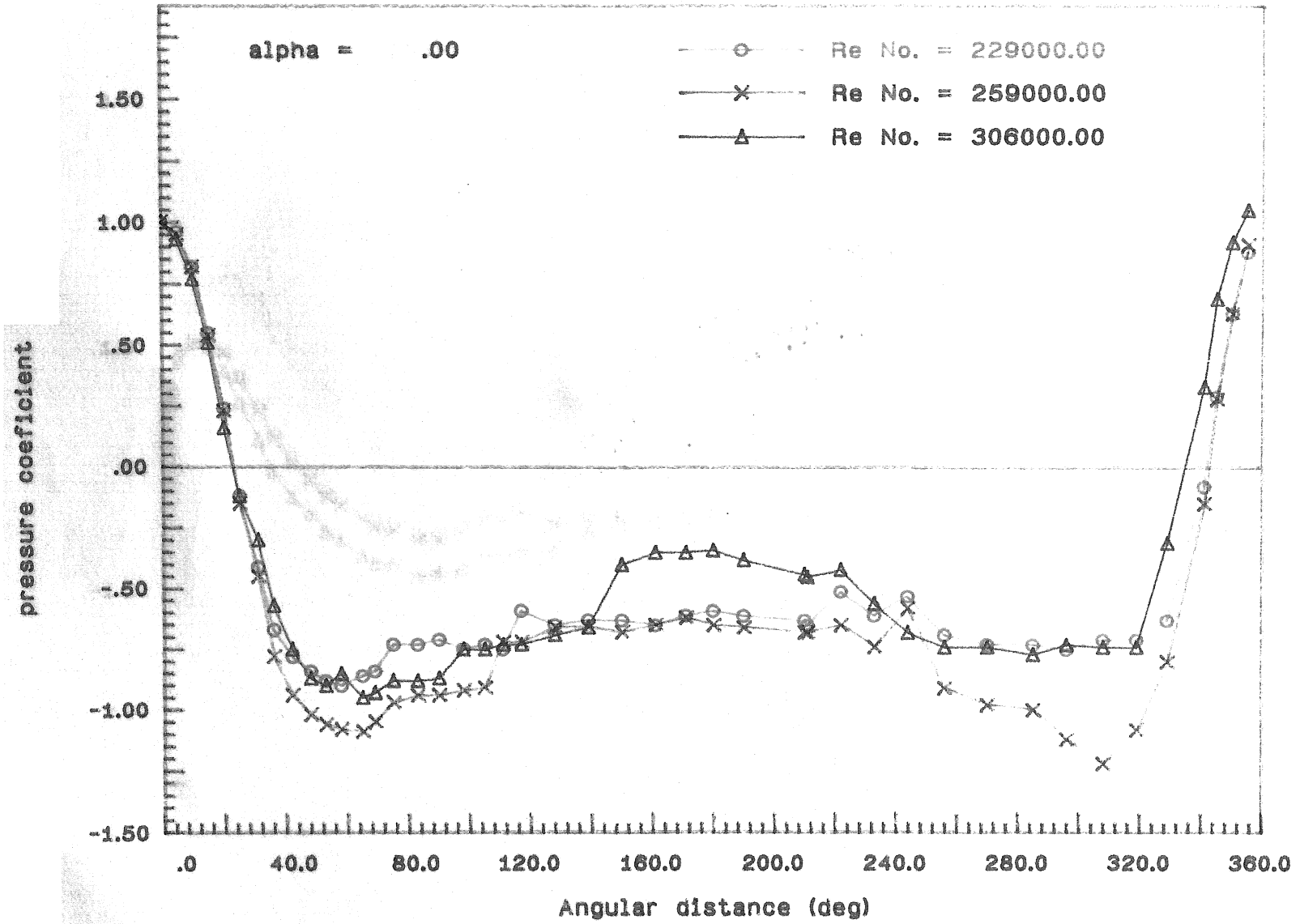

Fig b.1 : Variation of pressure coefficient over the surface of an elliptical cross section cylinder

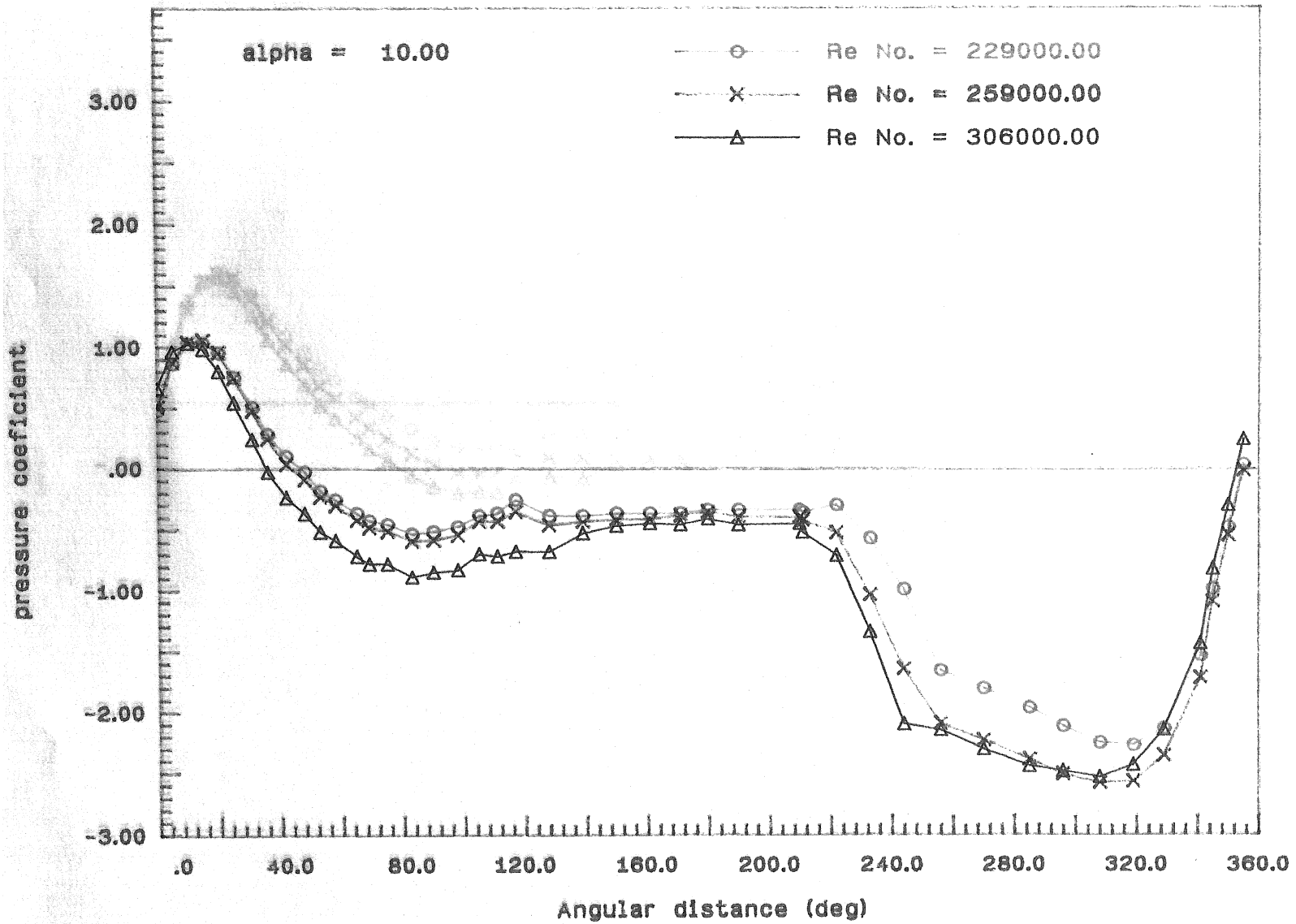

Fig b.2 : Variation of pressure coefficient over the surface of an elliptical cross section cylinder

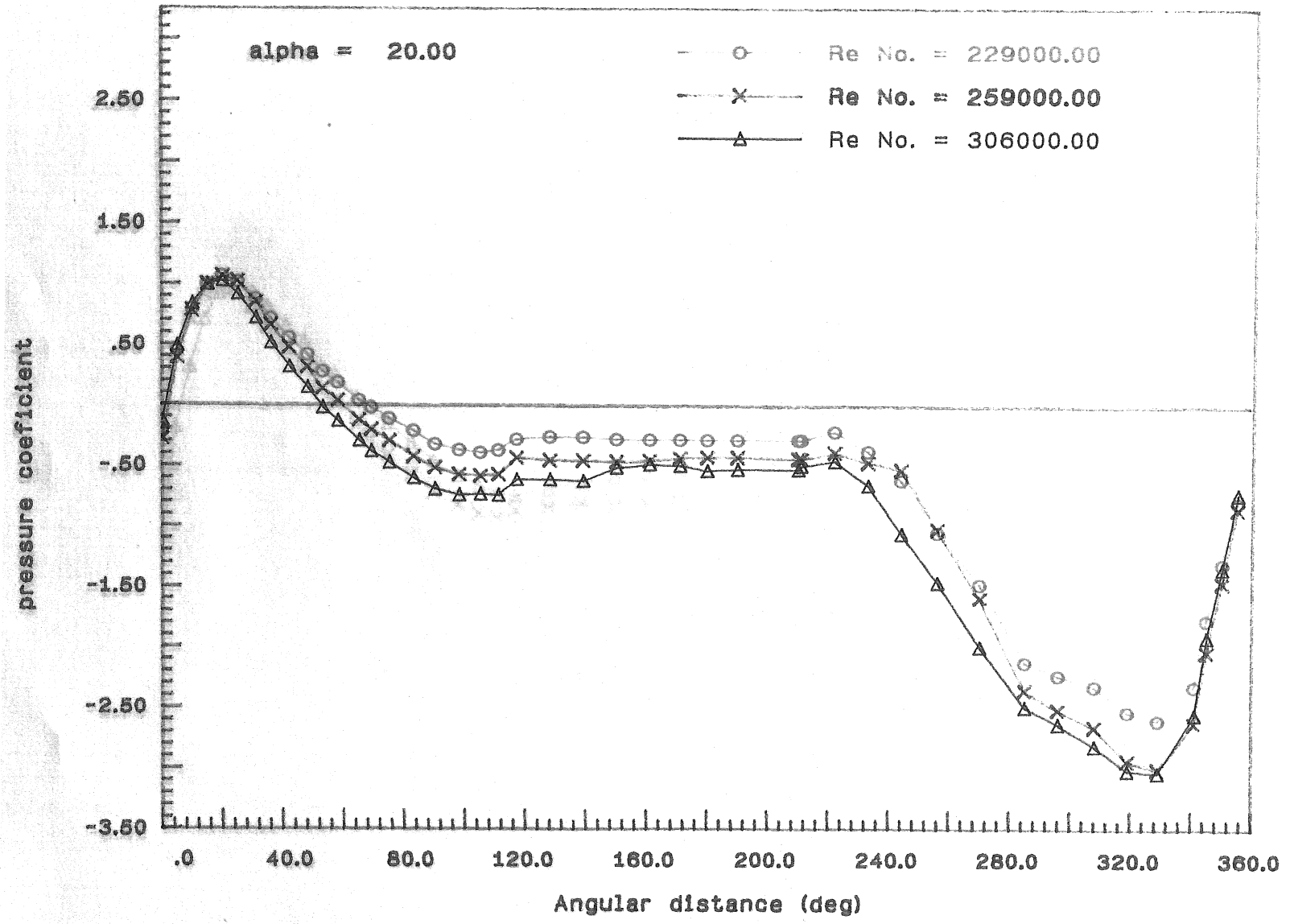

Fig b.3 : Variation of pressure coefficient over the surface of an elliptical cross section cylinder

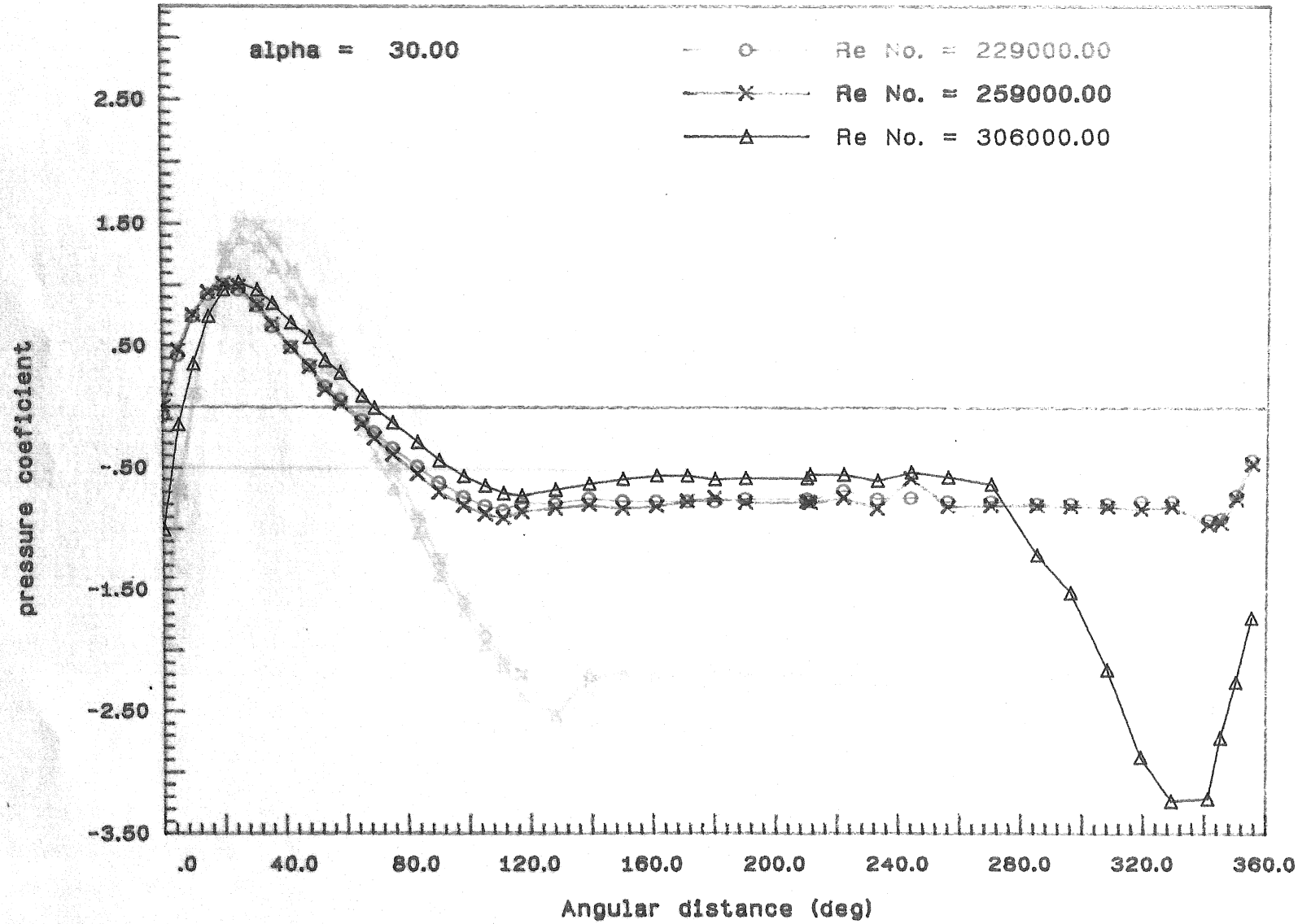

Fig b.4 : Variation of pressure coefficient over the surface of an elliptical cross section cylinder

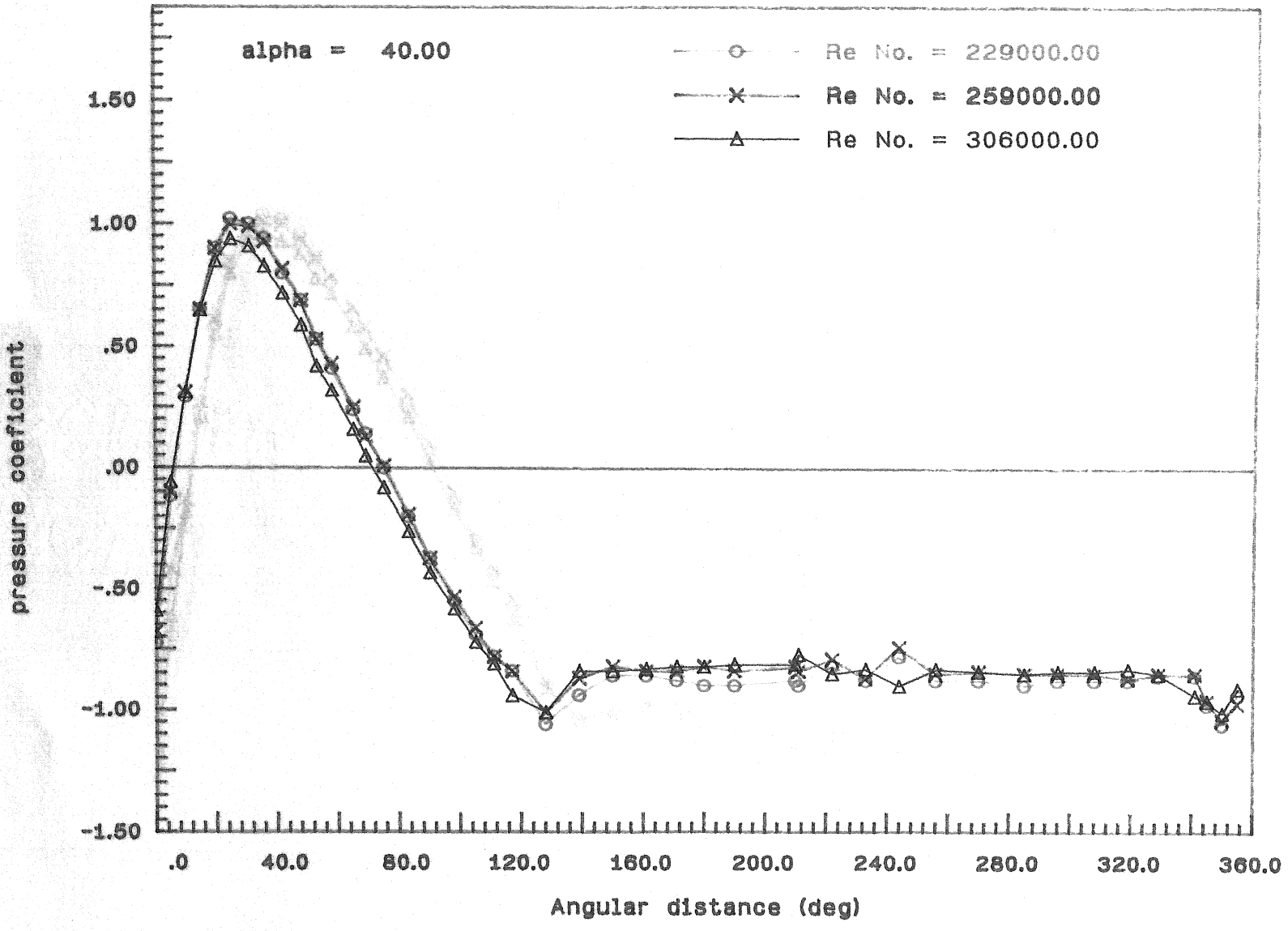

Fig b.5 : Variation of pressure coefficient over the surface of an elliptical cross section cylinder

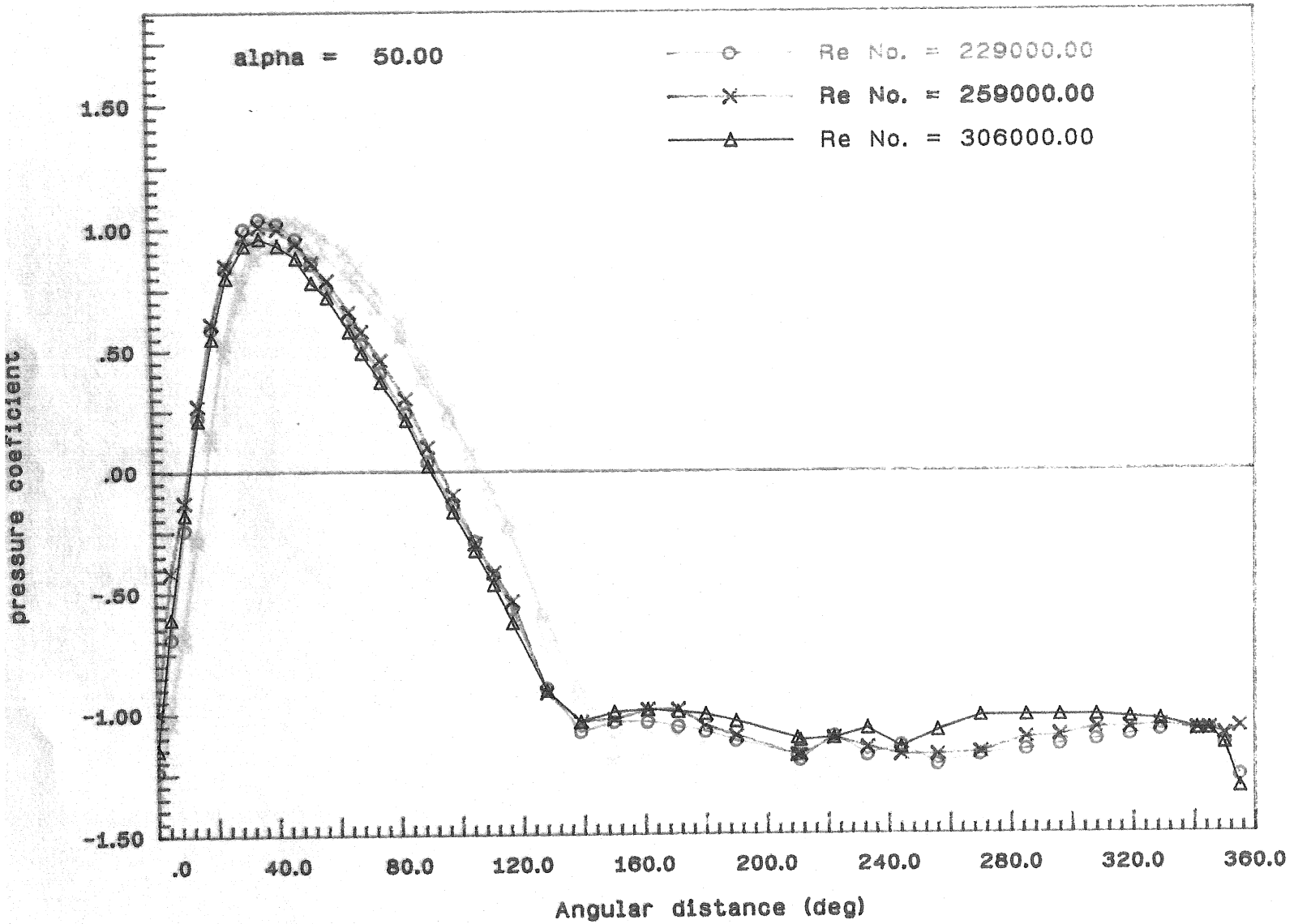

Fig b.6 : Variation of pressure coefficient over the surface of an elliptical cross section cylinder

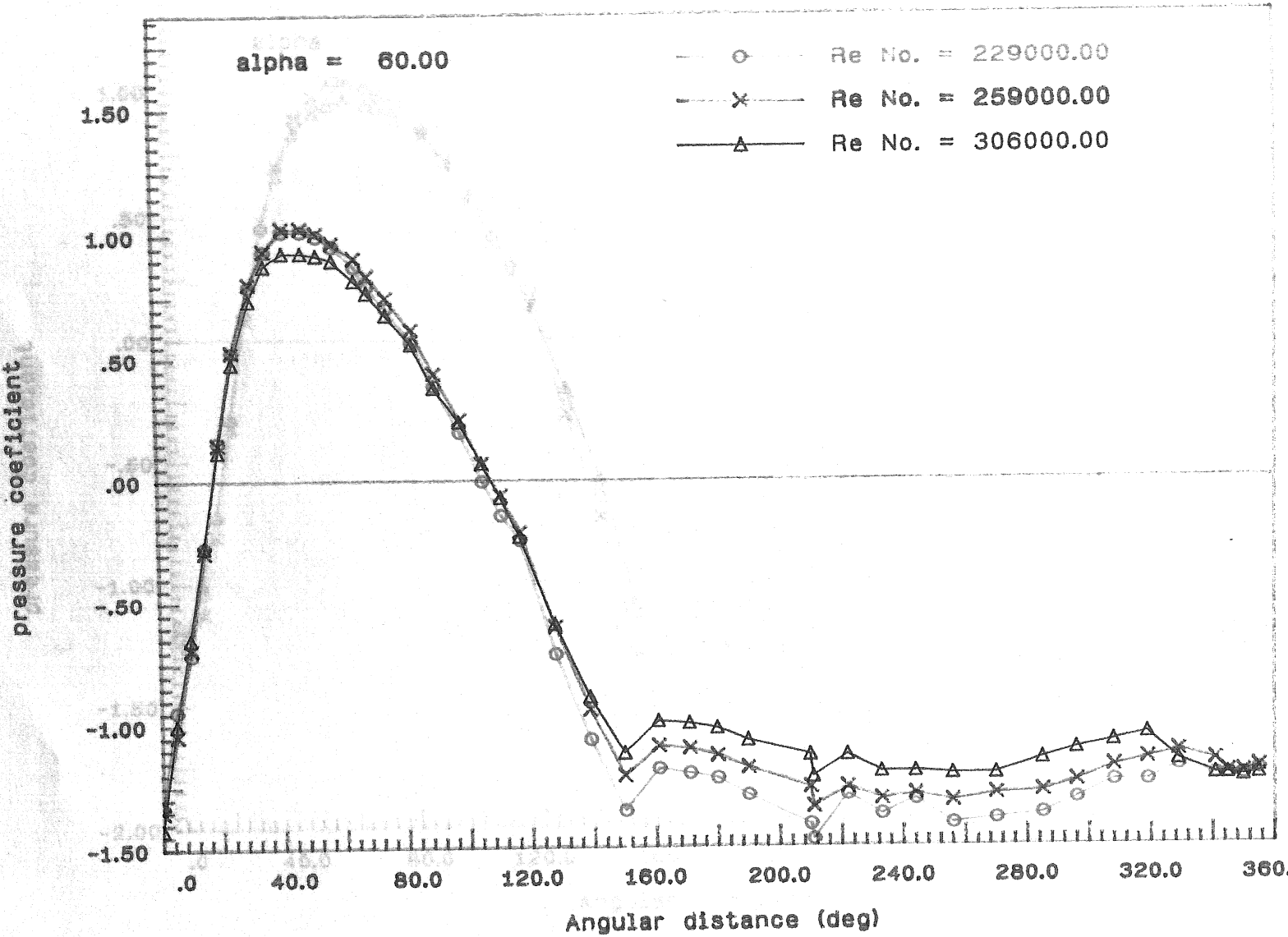

Fig b.7 : Variation of pressure coefficient over the surface of an elliptical cross section cylinder

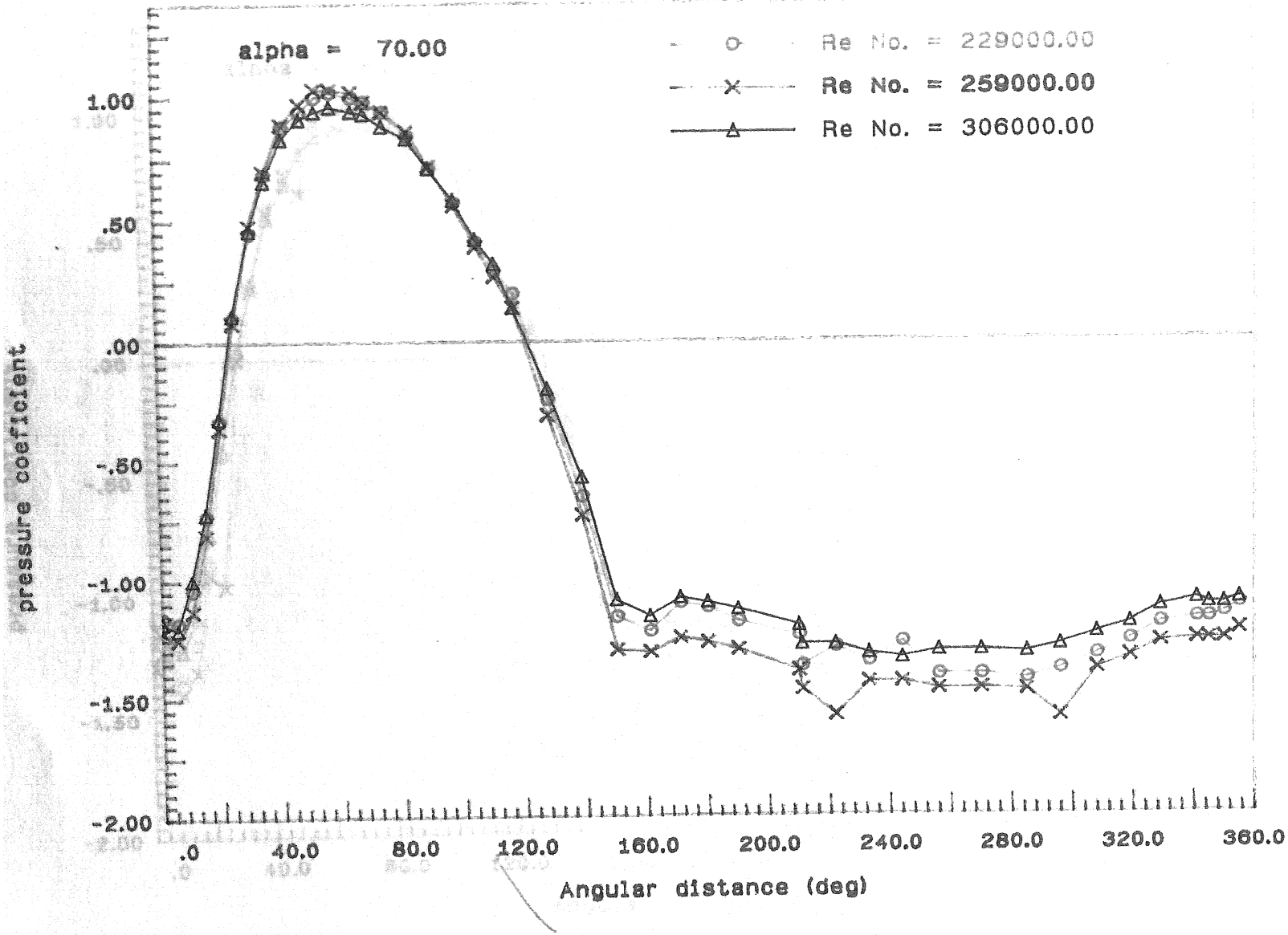

Fig b.8 : Variation of pressure coefficient over the surface of an elliptical cross section cylinder

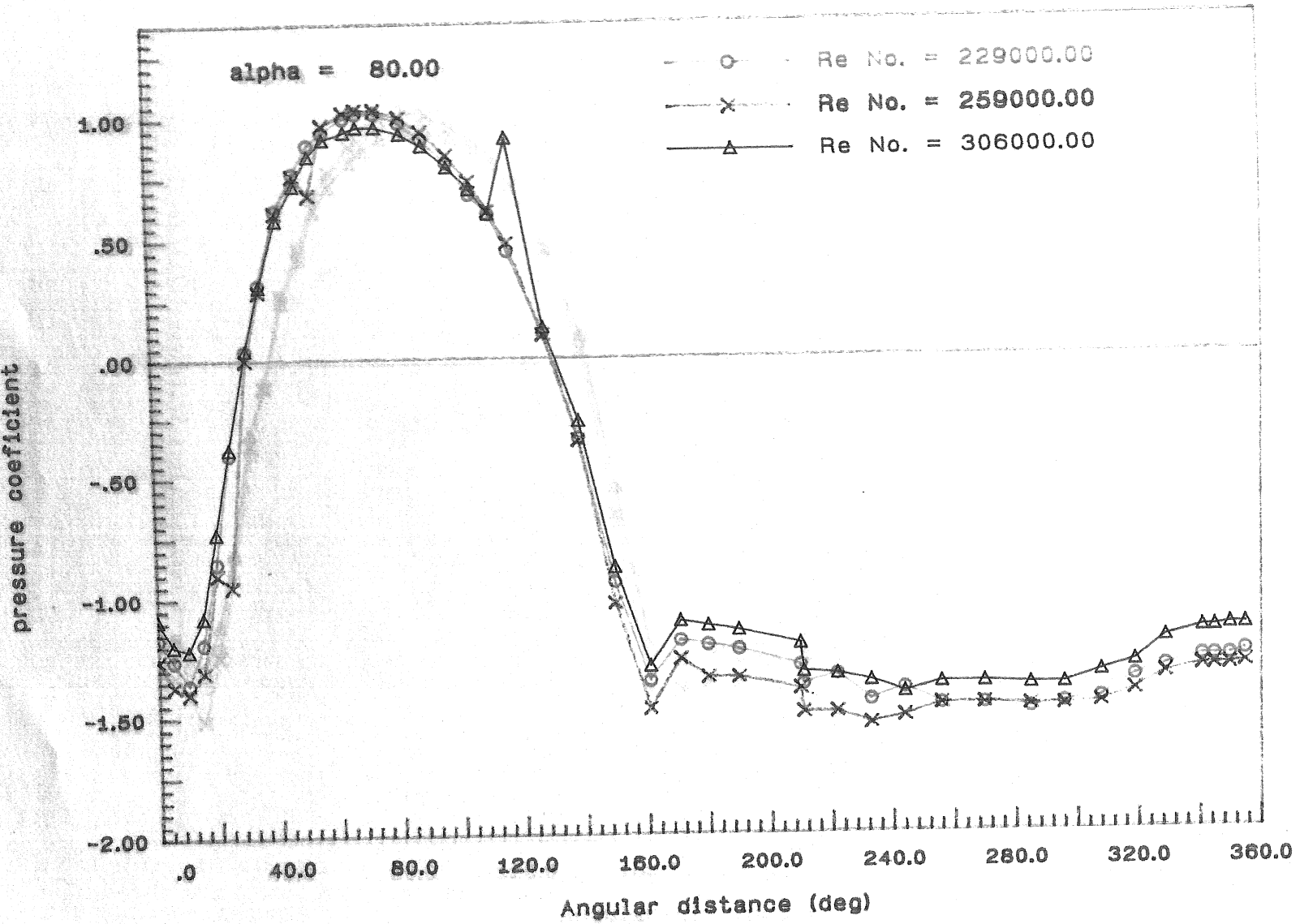

Fig b.9 : Variation of pressure coefficient over the surface of an elliptical cross section cylinder

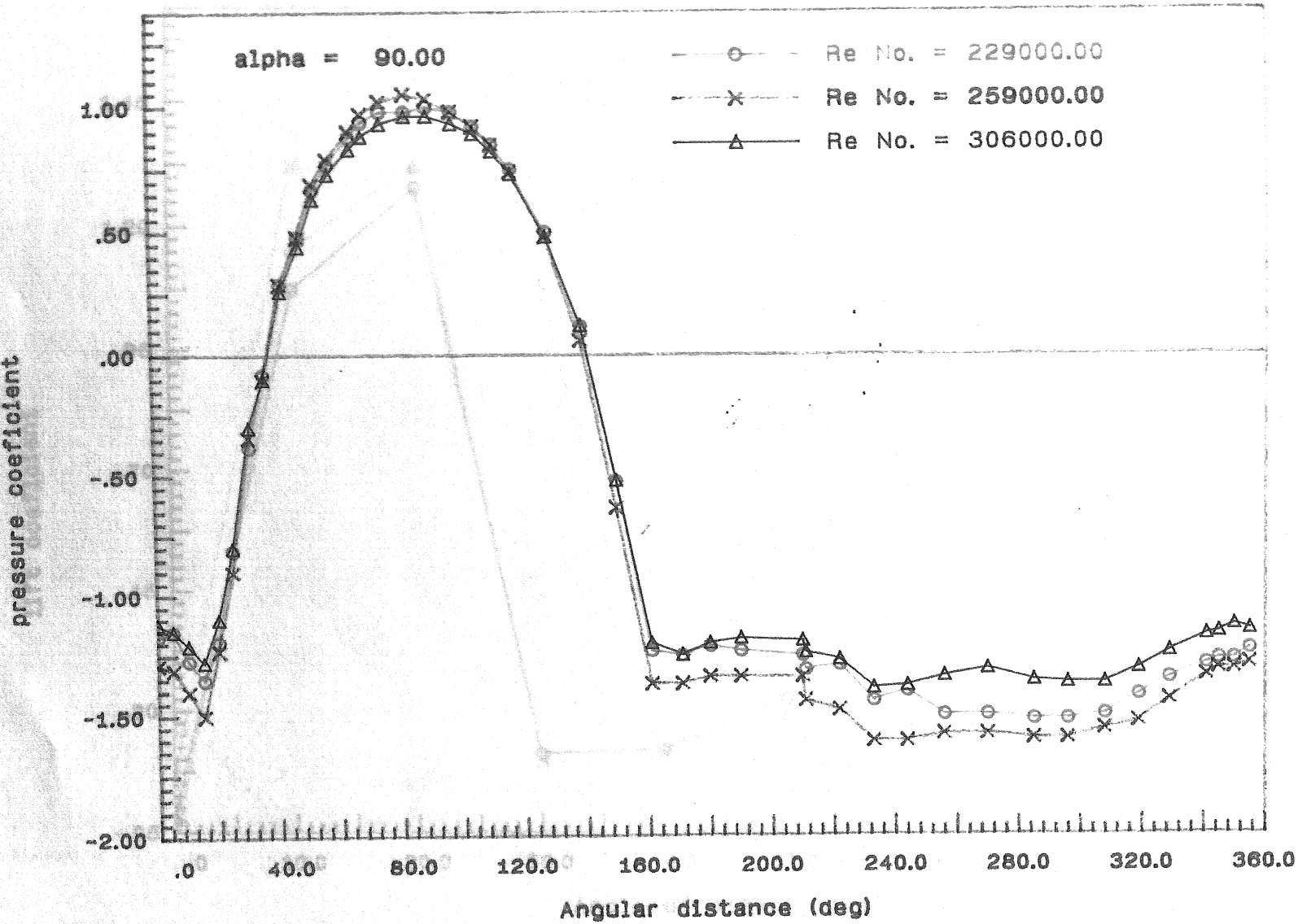

Fig b.10 : Variation of pressure coefficient over the surface of an elliptical cross section cylinder

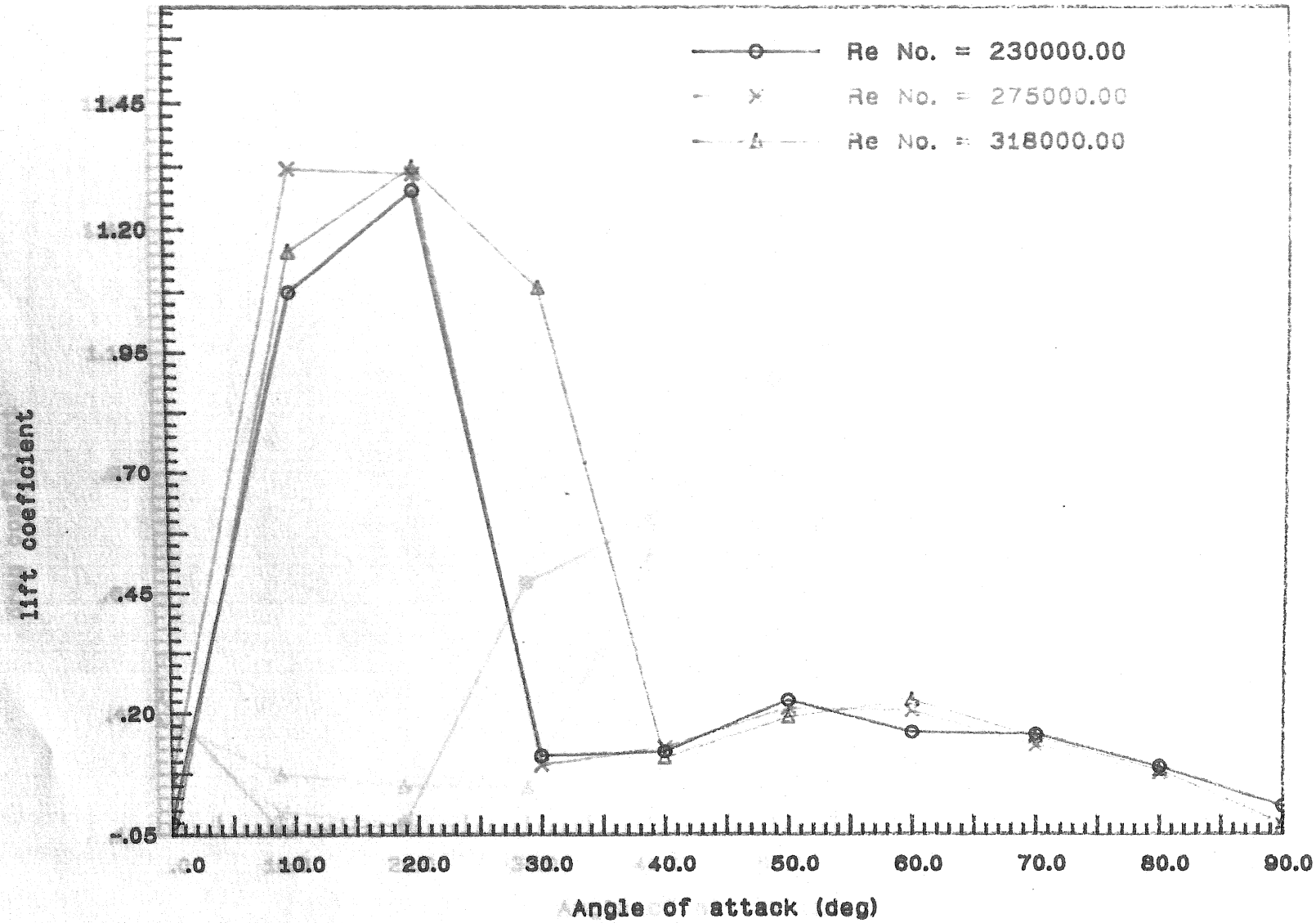

Fig b.11 : Variation of lift coefficient with angle of attack for an elliptical cylinder

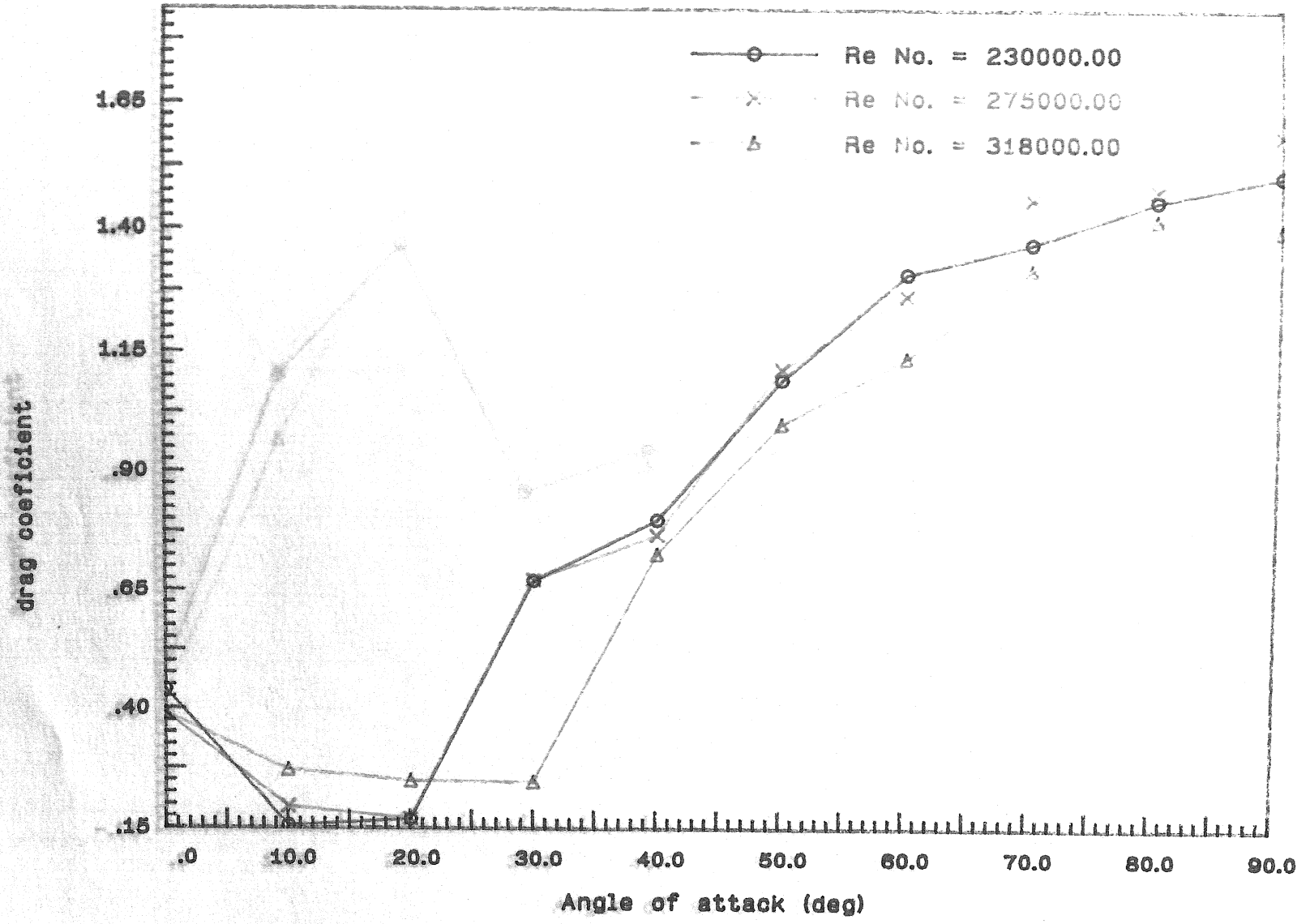

Fig b.12 : Variation of drag coefficient with angle of attack for an elliptical cylinder

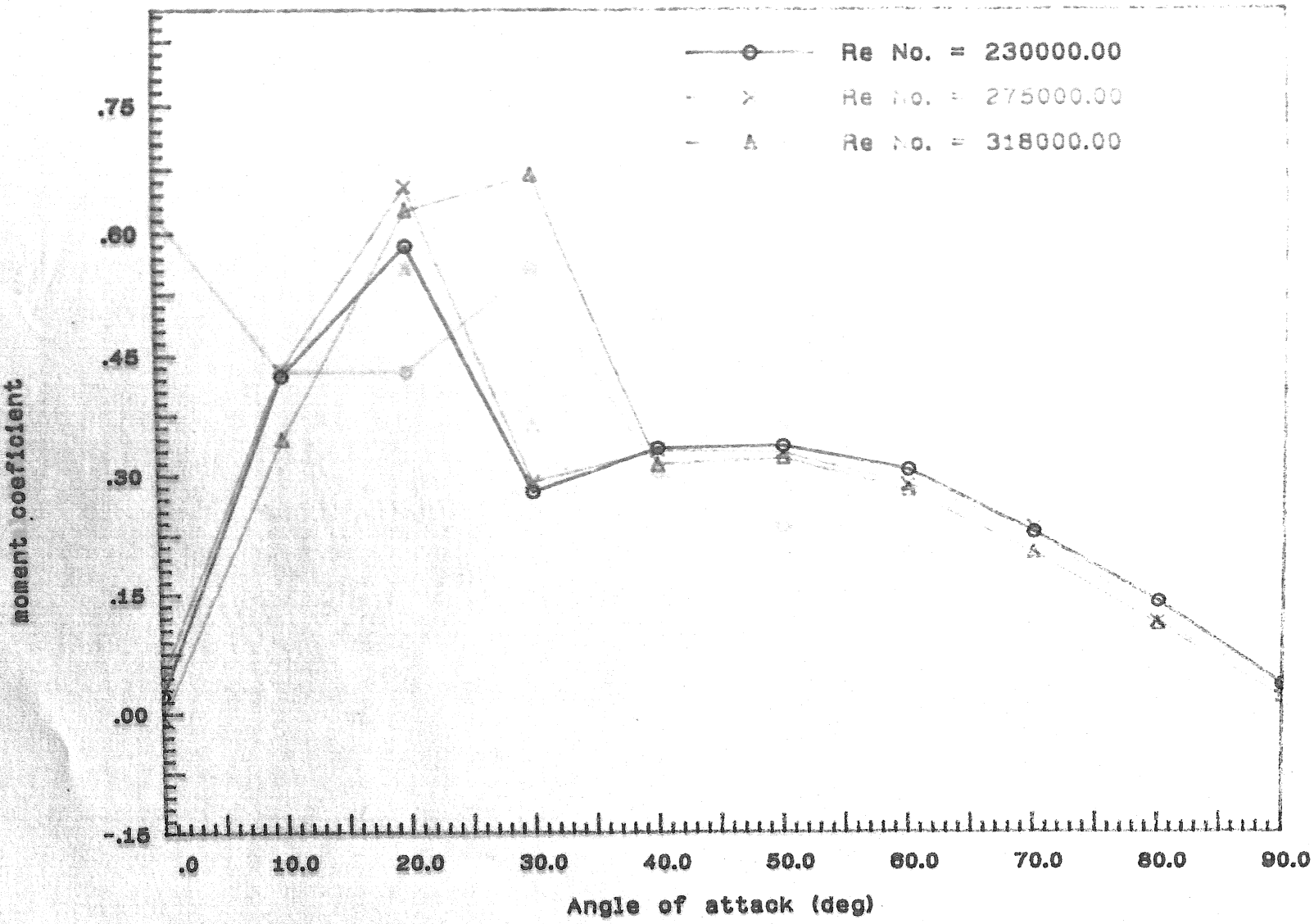

Fig b.13 : Variation of moment coefficient with angle of attack for an elliptical cylinder

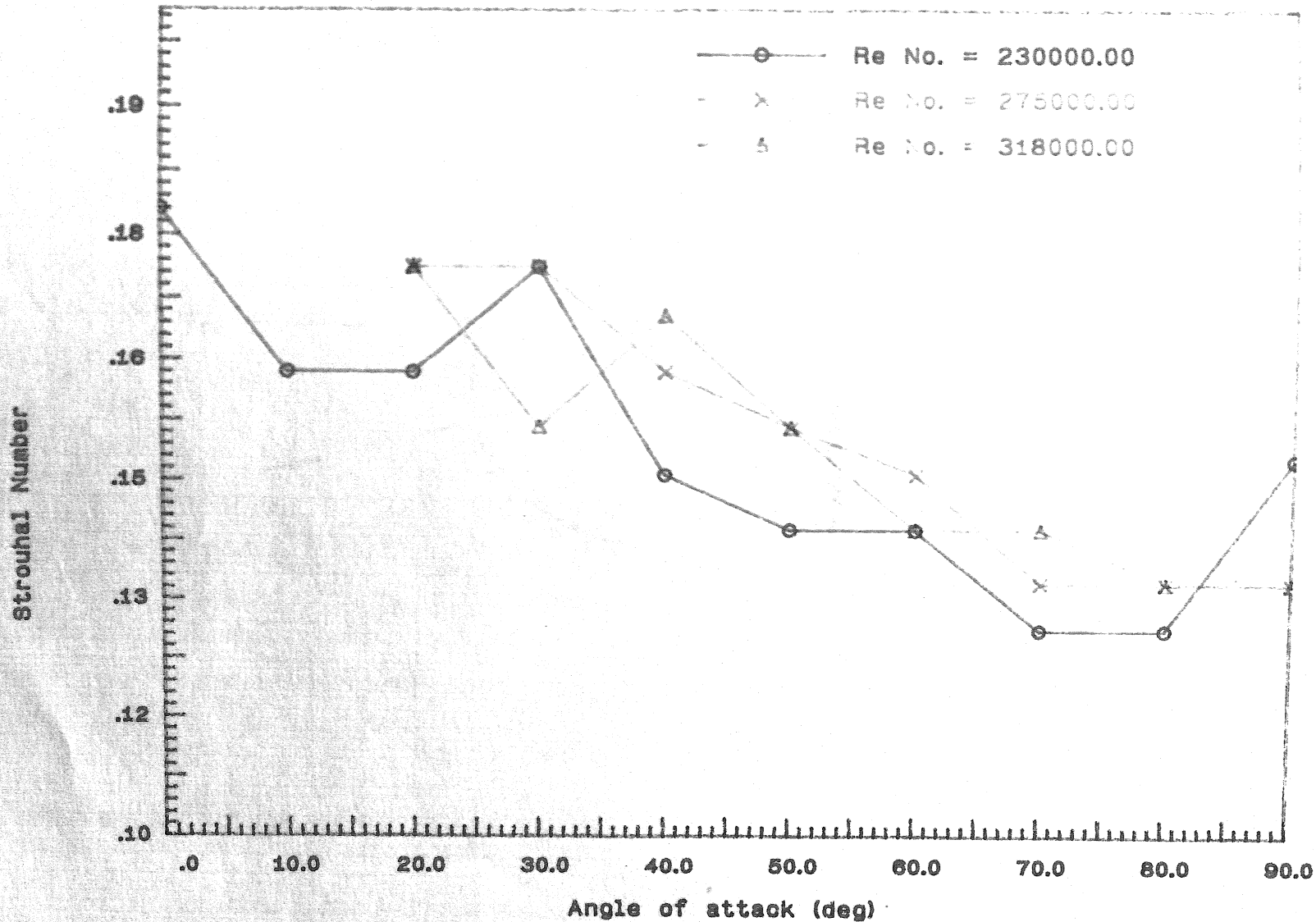

Fig b.14 : Variation of Strouhal Number with angle of attack for an elliptical cylinder

APPENDIX A

fig A.1

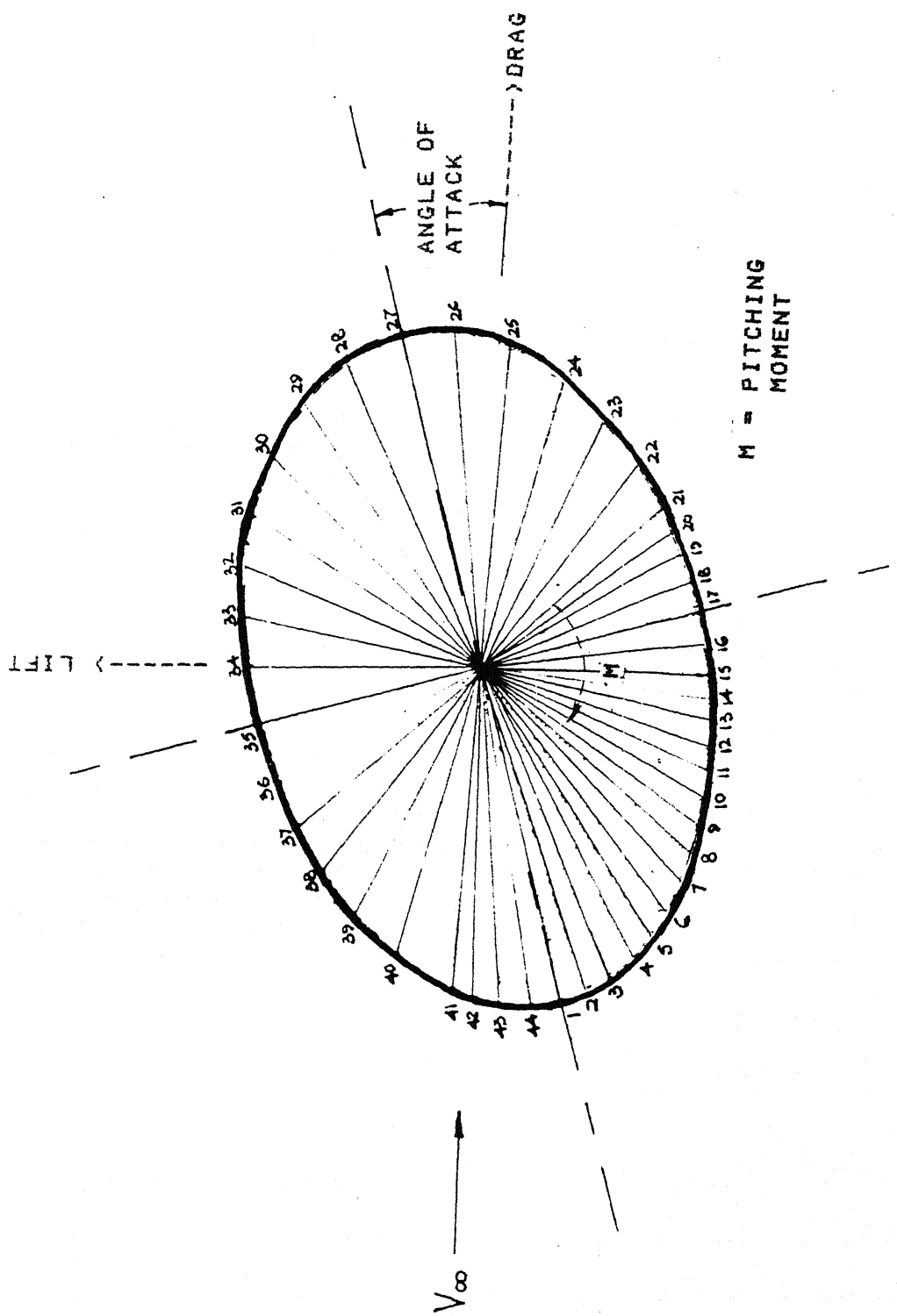

TABLE A2

Pressure Tap Point	Angular Distance(deg)
1	0.00
2	5.00
3	10.00
4	15.00
5	20.00
6	25.00
7	31.00
8	36.00
9	42.00
10	48.00
11	53.00
12	58.00
13	65.00
14	69.00
15	75.00
16	83.00
17	90.00
18	98.00
19	105.00
20	111.00
21	117.00
22	128.00

Pressure Tap Point	Angular Distance(deg)
23	139.00
24	150.00
25	161.00
26	171.00
27	180.00
28	190.00
29	210.00
30	211.00
31	222.00
32	233.00
33	244.00
34	256.00
35	270.00
36	285.00
37	296.00
38	308.00
39	319.00
40	329.00
41	341.00
42	345.00
43	350.00
44	355.00

APPENDIX B

```
program prog( input, output);

    const
        pi = 3.14159265;
    type
        vect = array [1..44] of real;
    var
        i, prev, next,j : integer;
        theta, alpha, b, e, c, d, s_9, s_10,s_11 : real;
        theta_2, h : vect;
        table : array [1..14, 1..44] of real;

    function sq( x : real) : real;
        begin
            sq := x * x;
        end;

    function tan( x :real) :real;
        begin
            tan := sin( x)/cos( x);
        end;

    begin
        for i := 1 to 44 do
            readln( table[1,i]);
        readln( alpha, c, d);
        b := c;
        e := (1.9-c);
        for i := 1 to 44 do
            readln( table[2,i]);
        for i := 1 to 44 do
            readln( table[3,i]);
        for i := 1 to 44 do
            table[4,i] := (180.0*arctan( 1.5*tan((pi*table[1,i])/ 180.0))/pi);
        for i:=1 to 16 do
            table[12,i] := table[4,i] +180.0;
        for i:=17 to 26 do
            table[12,i] := table[4,i] +360.0;
        for i:=27 to 35 do
            table[12,i] := table[4,i]+360.0;
        for i:=36 to 44 do
            table[12,i] := table[4,i] +540.0;
        for i := 1 to 44 do
            table[5,i] := table[12, i] -alpha;
        for i := 1 to 44 do
            table[6,i] :=(table[3,i]- table[2, i]);
        for i := 1 to 44 do
            table[7, i] :=  (table[6, i]-e)/ b;
        for i := 2 to 43 do
            begin
                prev := i -1;
                next := i +1;
                table[8, i] := (table[1, next] - table[1, prev])/2.0;
            end;
                table[8, 1] := 5.0;
                table[8, 44] := 5.0;
```

```
    for i := 1 to 44 do
        begin
            theta := ( table[1, i] * pi)/ 180.0;
            table[9, i] :=0.5* table[8, i] * sqrt( 10.5*10.5*
            sq( cos( theta))  + 49 * sq( sin( theta))) * pi/180.0;
        end;
    for i := 1 to 44 do
        table[ 10, i] :=-table[6, i]*
              table[ 9, i] * sin( (pi * table[ 5, i])/180.0);
    for i := 1 to 44 do
        table[ 11, i] :=-table[6,i]*
             table[ 9, i] * cos( ( pi * table[ 5, i])/180.0);
    for i:=1 to 44 do
        table[13,i] :=-((table[6,i]*table[ 9,i] *
       cos(( pi * table[12,i])/180.0)*(sin(( pi * table[1,i])/180.0))*7.0)
       -(table[6,i]*table[9,i] * sin(( pi * table[ 12,i])/180.0)*
       (cos(( pi * table[1,i])/180.0))*10.5));
    for i:=1 to 44 do
        table[14,i] :=table[1,i] -180.0;
    s_9 := 0.0;
    s_10 := 0.0;
    s_11 := 0.0;
    for i := 1 to 44 do
        begin
          s_9 := s_9 + table[ 10, i];
          s_10 := s_10 + table[ 11, i];
          s_11 := s_11 + table[ 13,i];
        end;
    s_9 := s_9/(10.5* b);
    s_10 := s_10/(10.5*b);
    s_11 := s_11/(10.5*b*7.0);
    writeln( 'LIFT COEFFICIENT = ', s_9:15:5);
    writeln( 'DRAG COEFFICIENT = ', s_10:15:5);
    writeln( 'MOMENT COEFFICIENT = ', s_11:15:5);

    for i:=1 to 44 do
    writeln(table[14,i]:10:2,table[7,i]:10:2);
end.
```

APPENDIX C

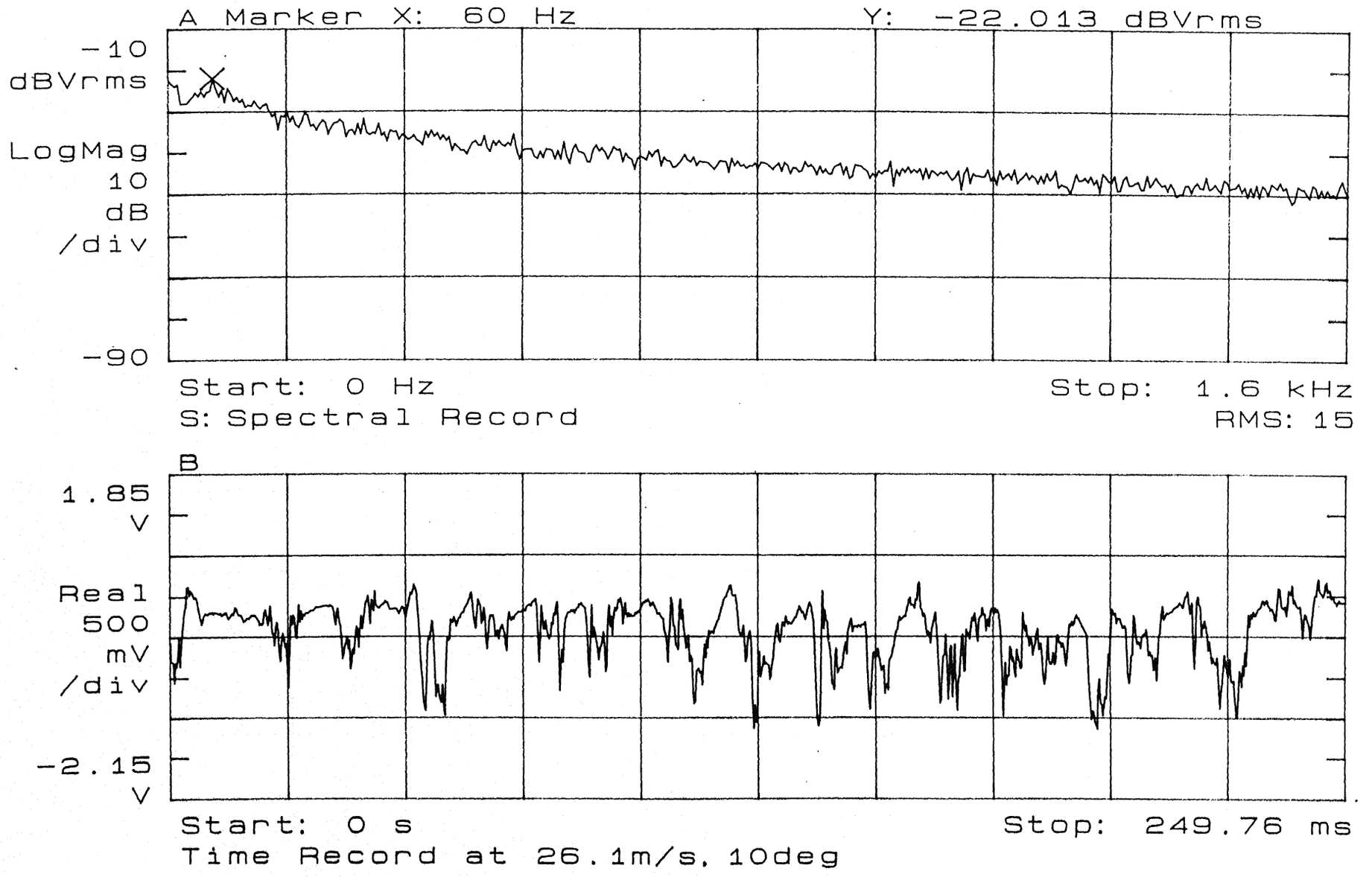
A Marker X: 60 Hz
Y: -22.013 dBVrms
-10
dBVrms
LogMag
10
dB
/div
-90
Start: 0 Hz
Stop: 1.6 kHz
S: Spectral Record
RMS: 15
B
1.85
V
Real
500
mV
/div
-2.15
V
Start: 0 s
Stop: 249.76 ms
Time Record at 26.1m/s, 10deg

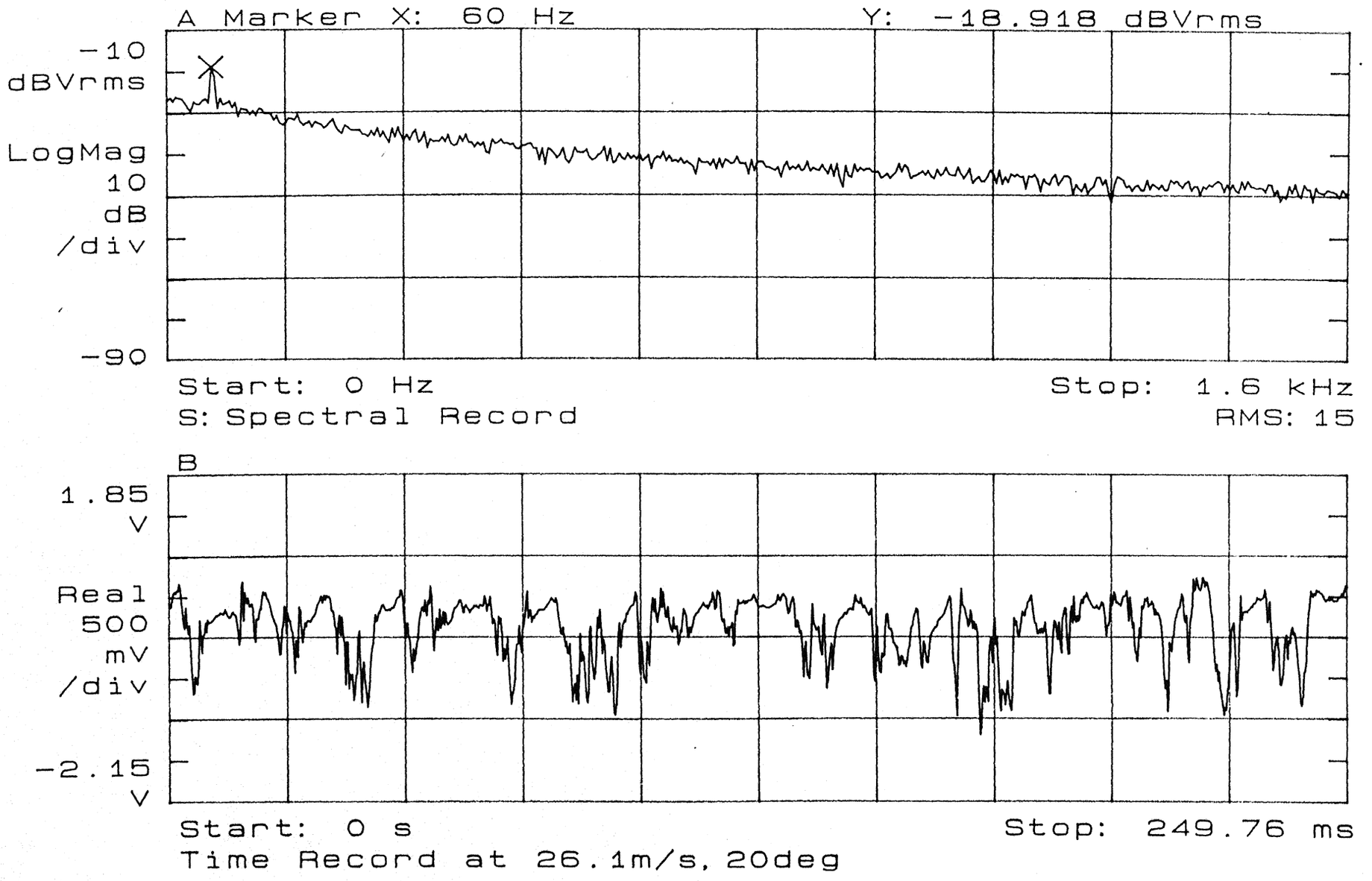
A Marker X: 60 Hz
Y: -18.918 dBVrms
-10
dBVrms
LogMag
10
dB
/div
-90
Start: 0 Hz
Stop: 1.6 kHz
S: Spectral Record
RMS: 15
B
1.85
V
Real
500
mV
/div
-2.15
V
Start: 0 s
Stop: 249.76 ms
Time Record at 26.1m/s, 20deg

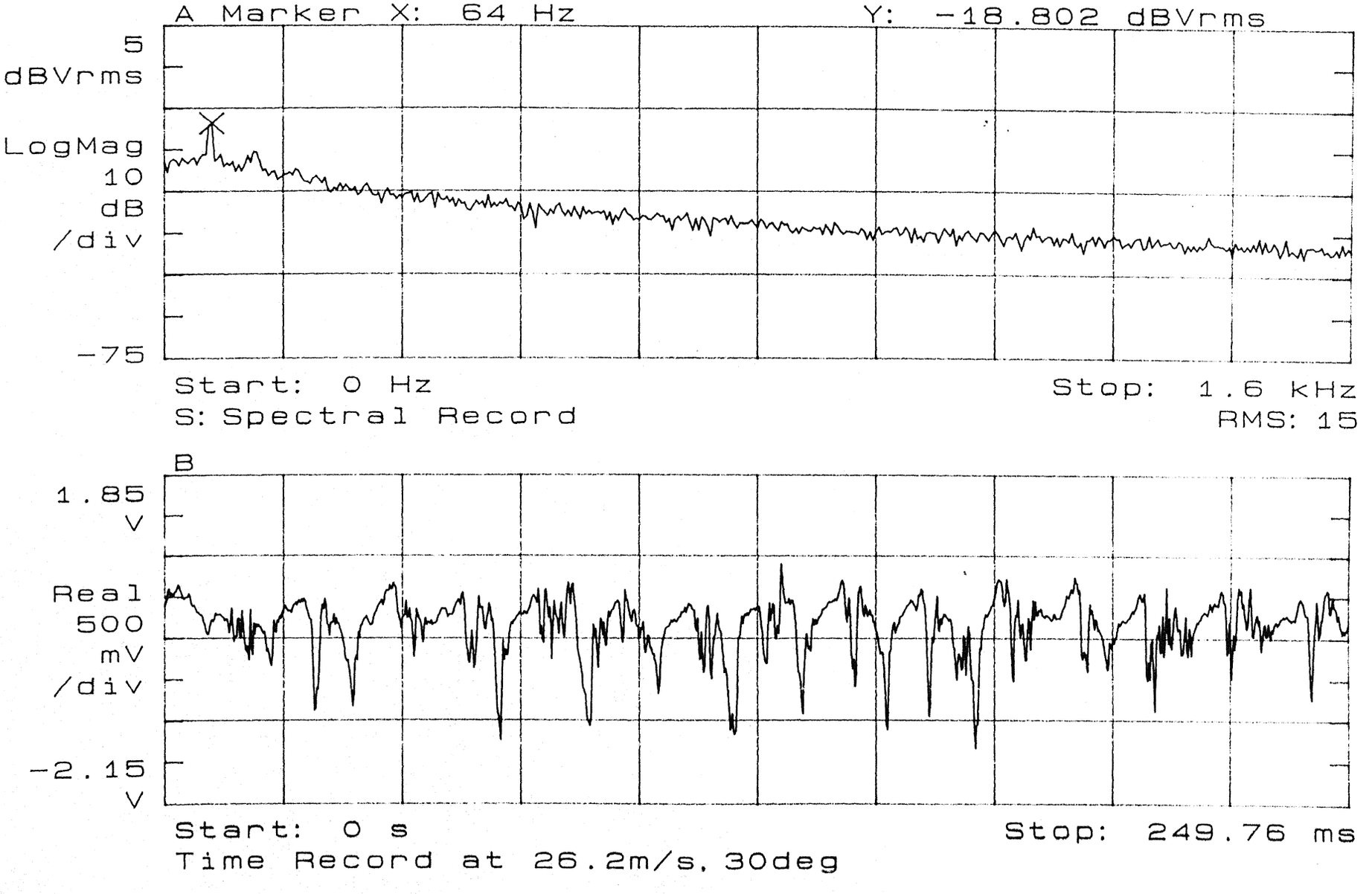
A Marker X: 64 Hz
Y: -18.802 dBVrms
5
dBVrms
LogMag
10
dB
/div
-75
Start: 0 Hz
Stop: 1.6 kHz
S: Spectral Record
RMS: 15
B
1.85
V
Real
500
mV
/div
-2.15
V
Start: 0 s
Stop: 249.76 ms
Time Record at 26.2m/s, 30deg

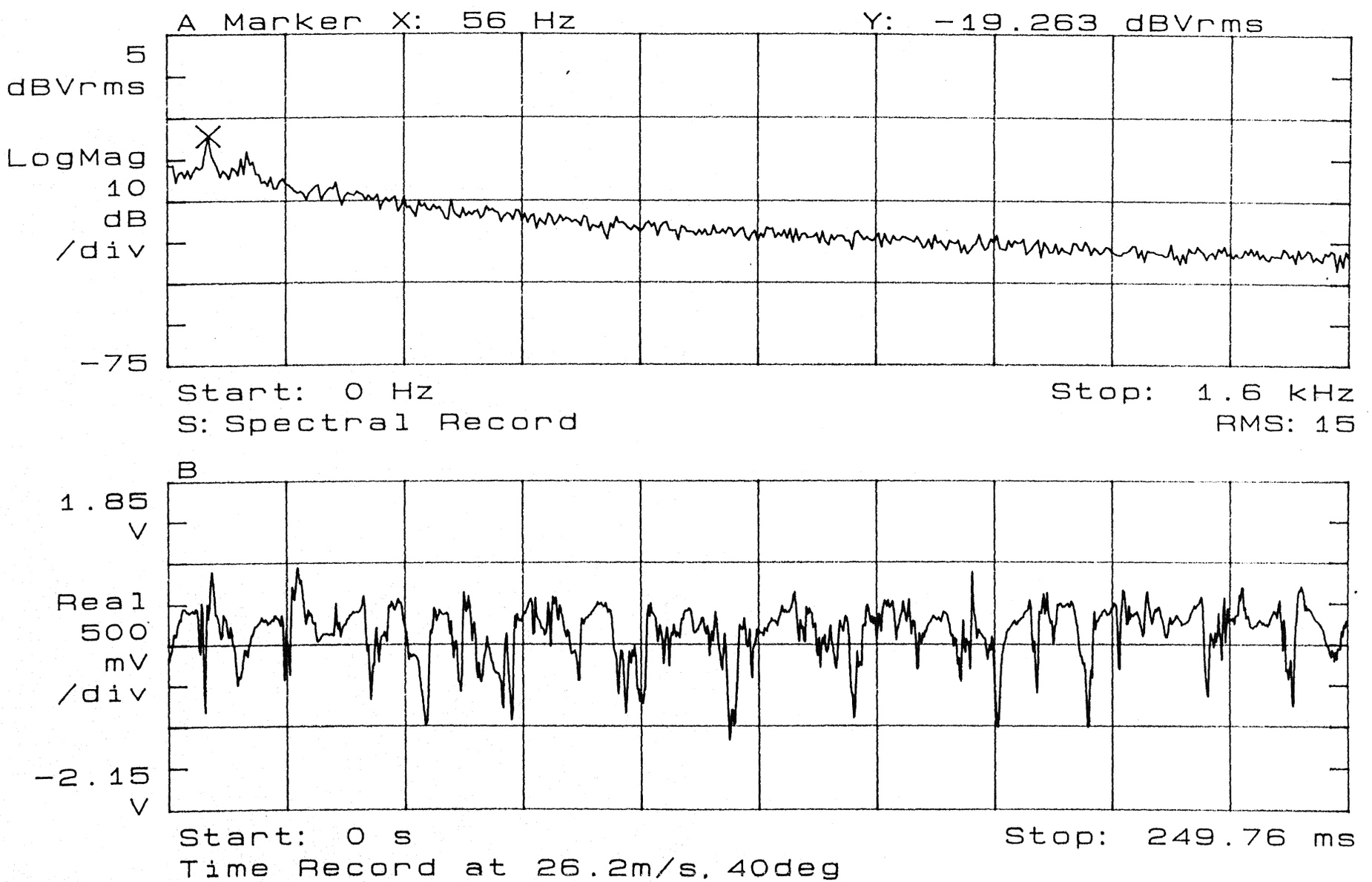
A Marker X: 56 Hz
Y: -19.263 dBVrms
5
dBVrms
LogMag
10
dB
/div
-75
Start: 0 Hz
Stop: 1.6 kHz
S: Spectral Record
RMS: 15
B
1.85
V
Real
500
mV
/div
-2.15
V
Start: 0 s
Stop: 249.76 ms
Time Record at 26.2m/s, 40deg

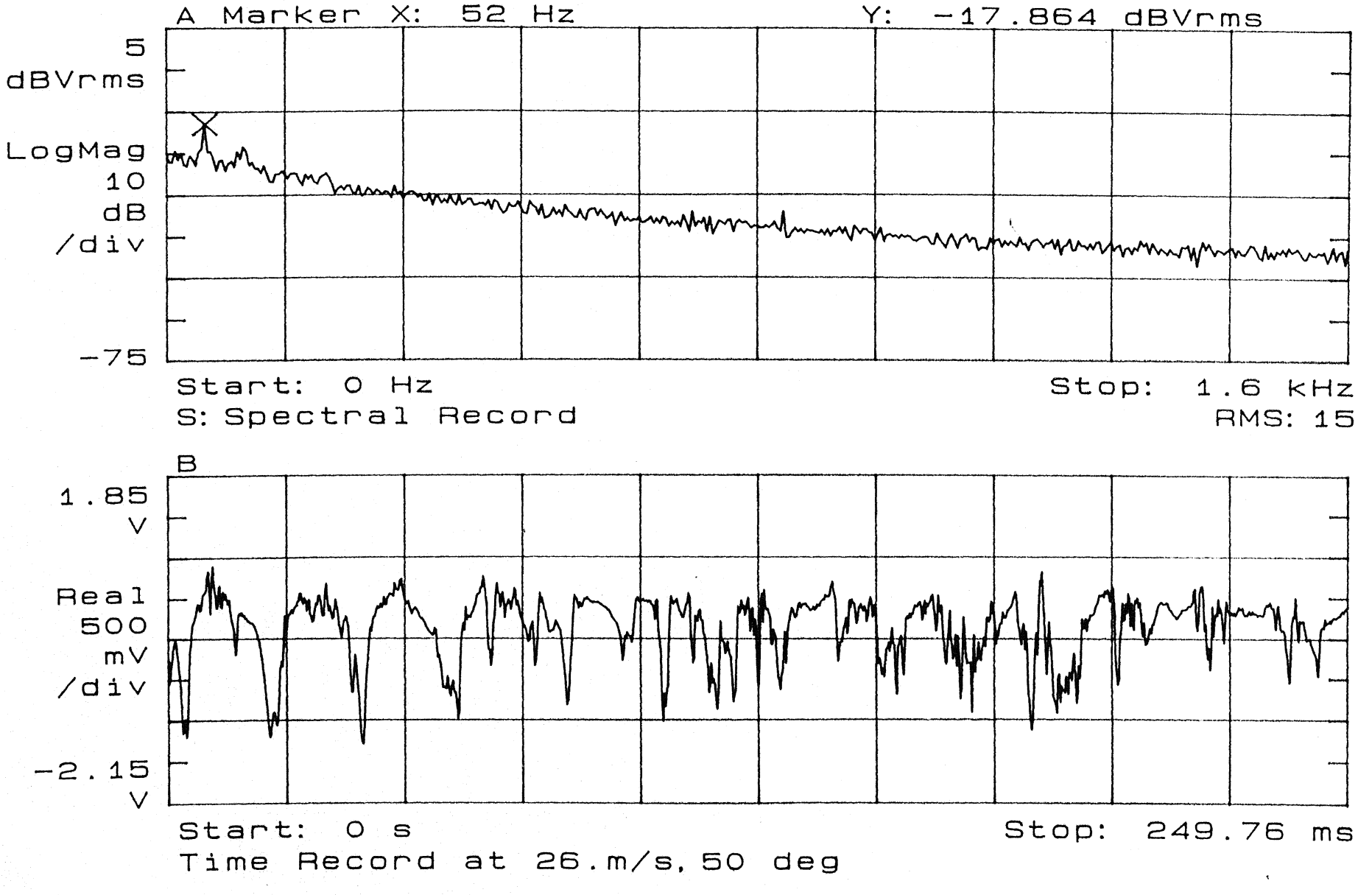
A Marker X: 52 Hz
Y: -17.864 dBVrms
5
dBVrms
LogMag
10
dB
/div
-75
Start: 0 Hz
Stop: 1.6 kHz
S: Spectral Record
RMS: 15
B
1.85
V
Real
500
mV
/div
-2.15
V
Start: 0 s
Stop: 249.76 ms
Time Record at 26.m/s, 50 deg

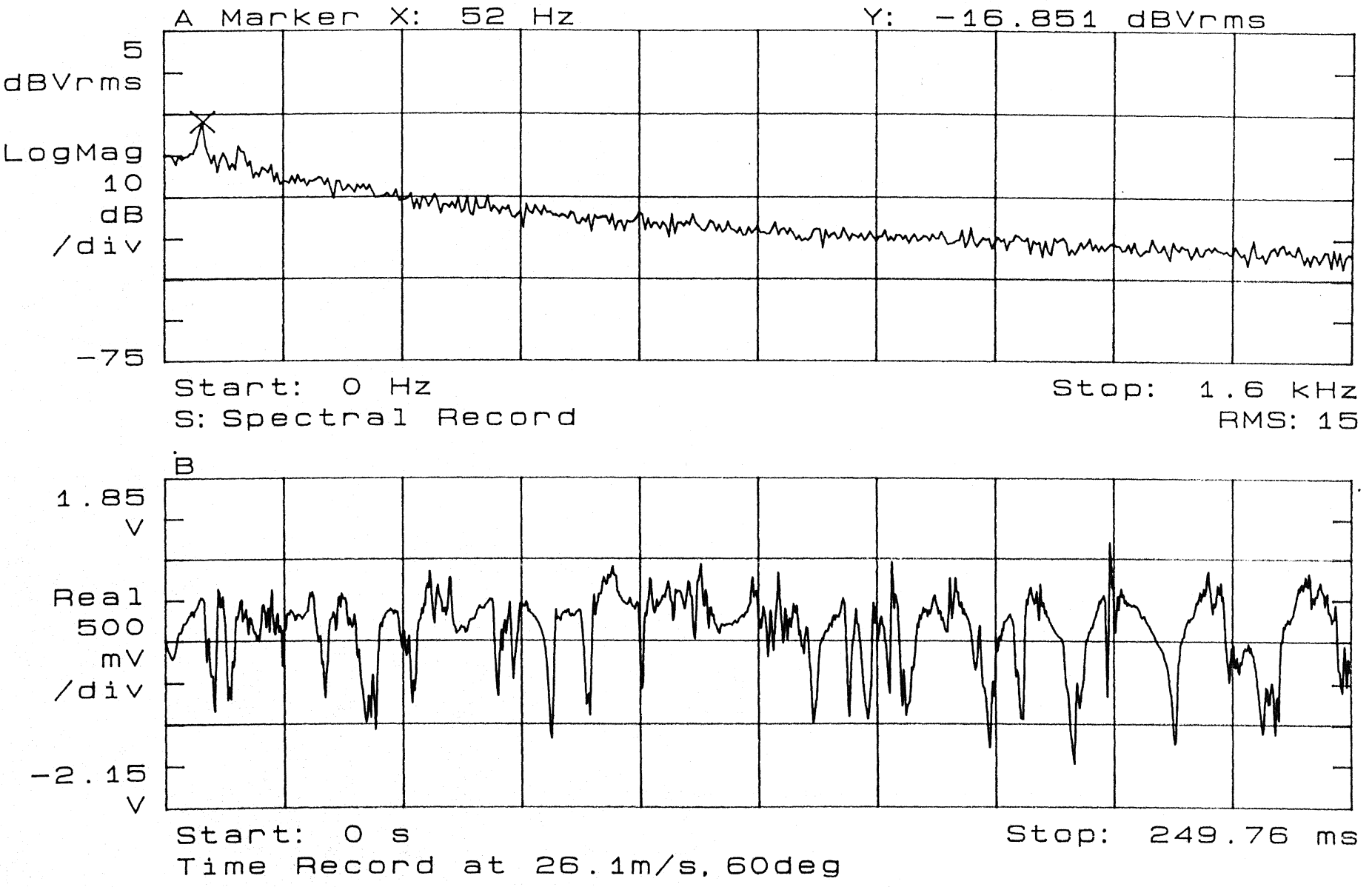
A Marker X: 52 Hz
Y: -16.851 dBVrms
5
dBVrms
LogMag
10
dB
/div
-75
Start: 0 Hz
Stop: 1.6 kHz
S: Spectral Record
RMS: 15
B
1.85
V
Real
500
mV
/div
-2.15
V
Start: 0 s
Stop: 249.76 ms
Time Record at 26.1m/s, 60deg

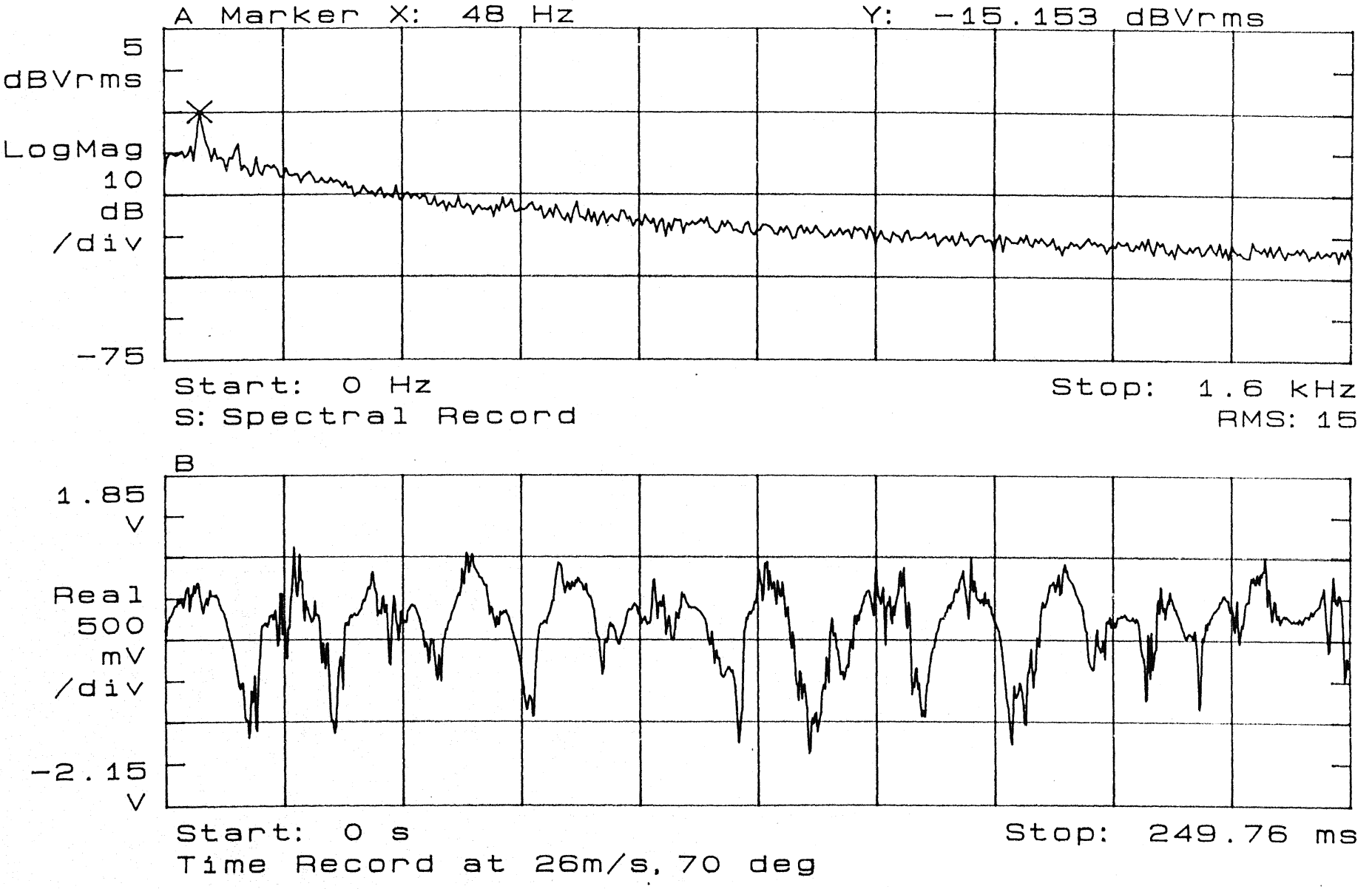
A Marker X: 48 Hz
Y: -15.153 dBVrms
5
dBVrms
LogMag
10
dB
/div
-75
Start: 0 Hz
Stop: 1.6 kHz
S: Spectral Record
RMS: 15
B
1.85
V
Real
500
mV
/div
-2.15
V
Start: 0 s
Stop: 249.76 ms
Time Record at 26m/s, 70 deg

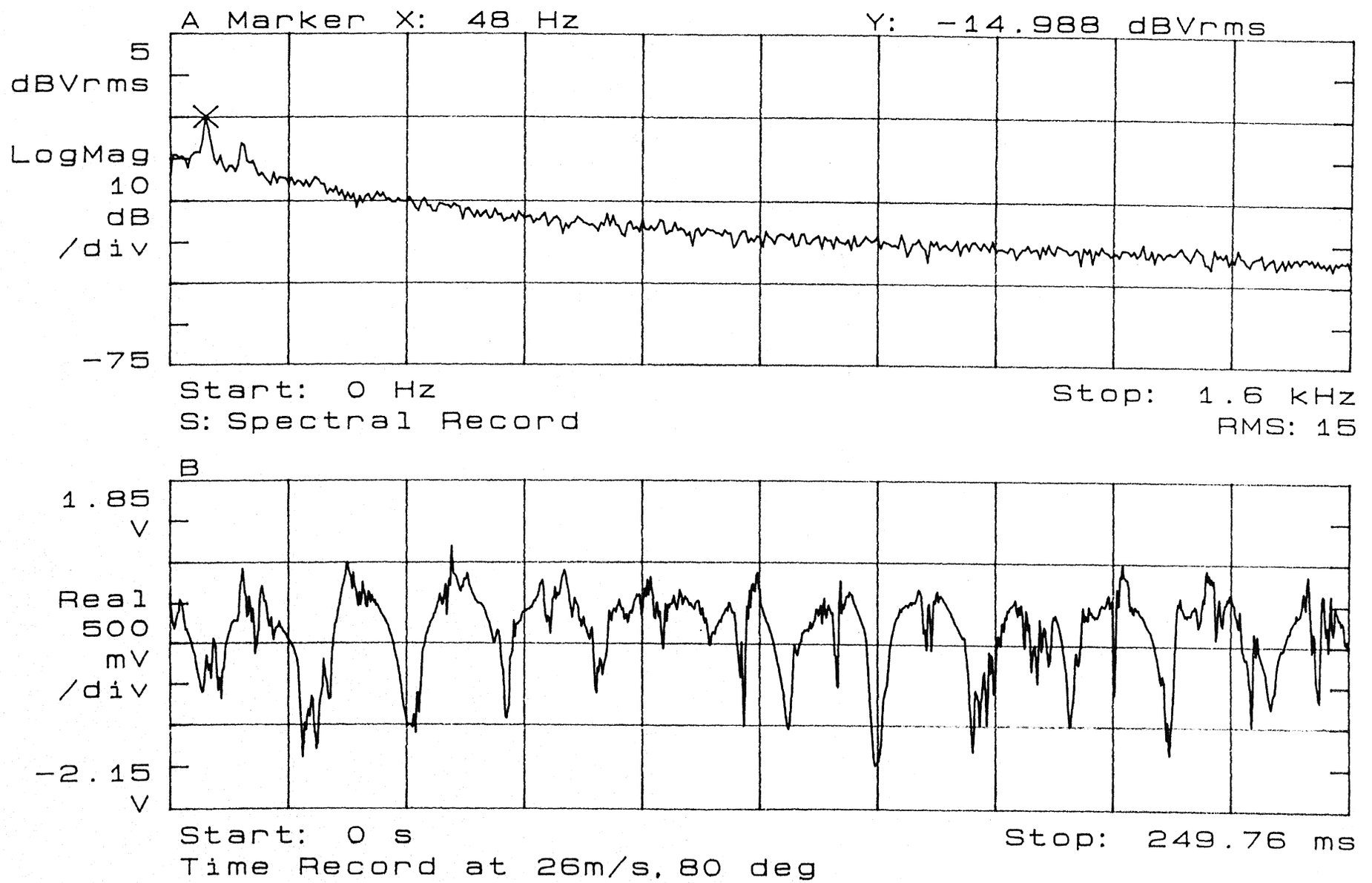
A Marker X: 48 Hz
Y: -14.988 dBVrms
5
dBVrms
LogMag
10
dB
/div
-75
Start: 0 Hz
Stop: 1.6 kHz
S: Spectral Record
RMS: 15
B
1.85
V
Real
500
mV
/div
-2.15
V
Start: 0 s
Stop: 249.76 ms
Time Record at 26m/s, 80 deg

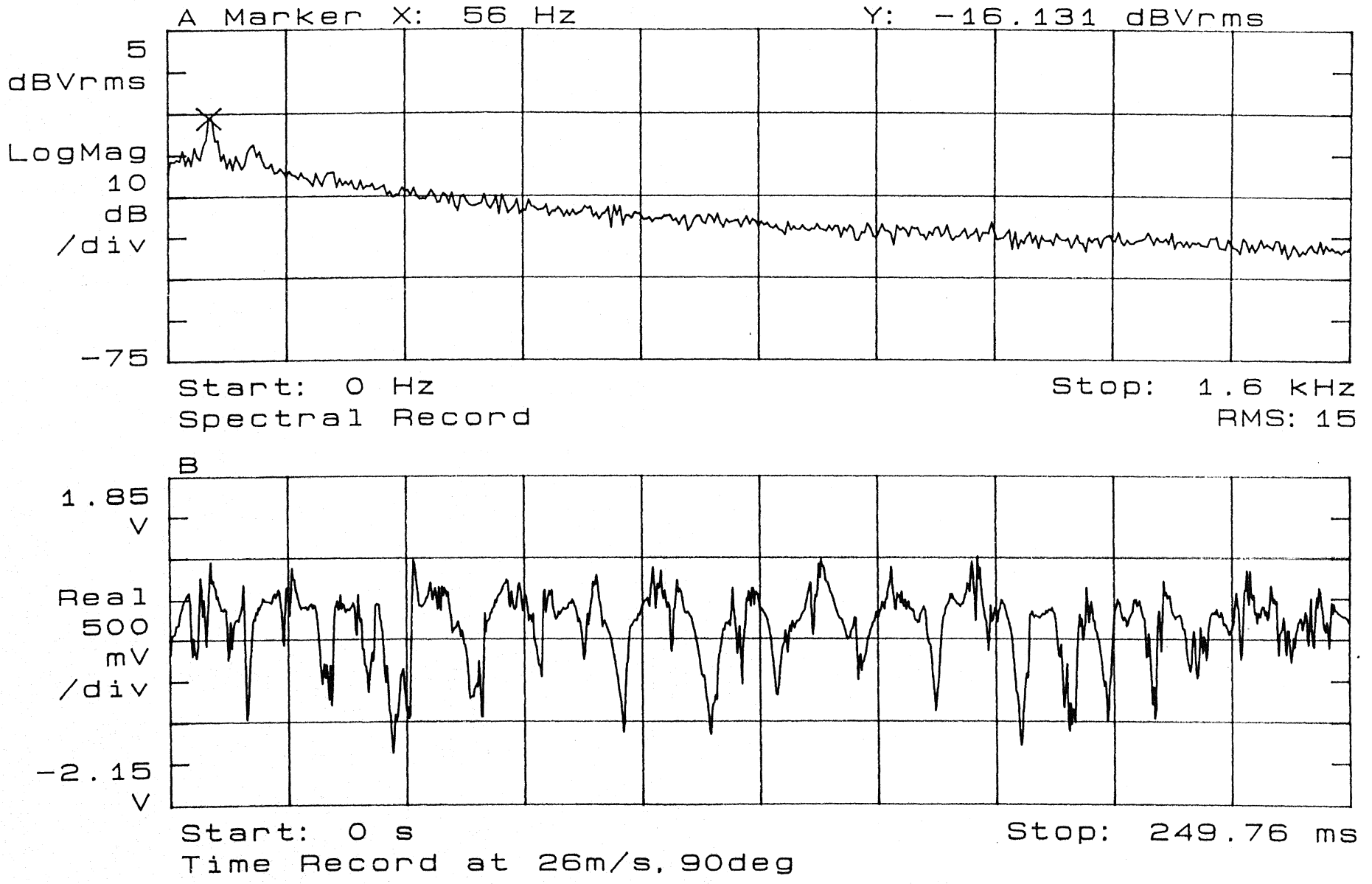
A Marker X: 56 Hz
Y: -16.131 dBVrms
5
dBVrms
LogMag
10
dB
/div
-75
Start: 0 Hz
Stop: 1.6 kHz
Spectral Record
RMS: 15
B
1.85
V
Real
500
mV
/div
-2.15
V
Start: 0 s
Stop: 249.76 ms
Time Record at 26m/s, 90deg

REAL-TIME AVG COMPLETE

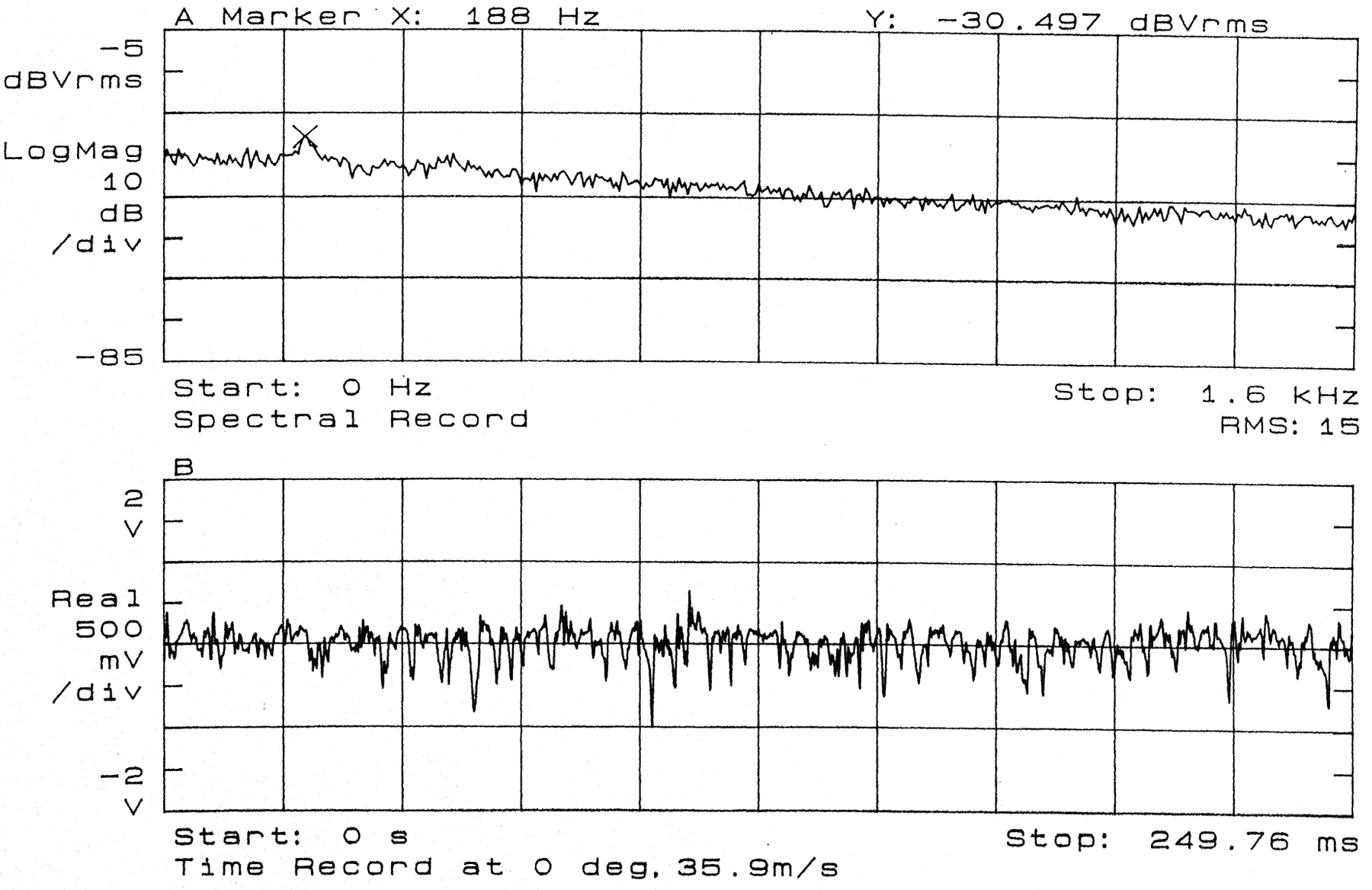

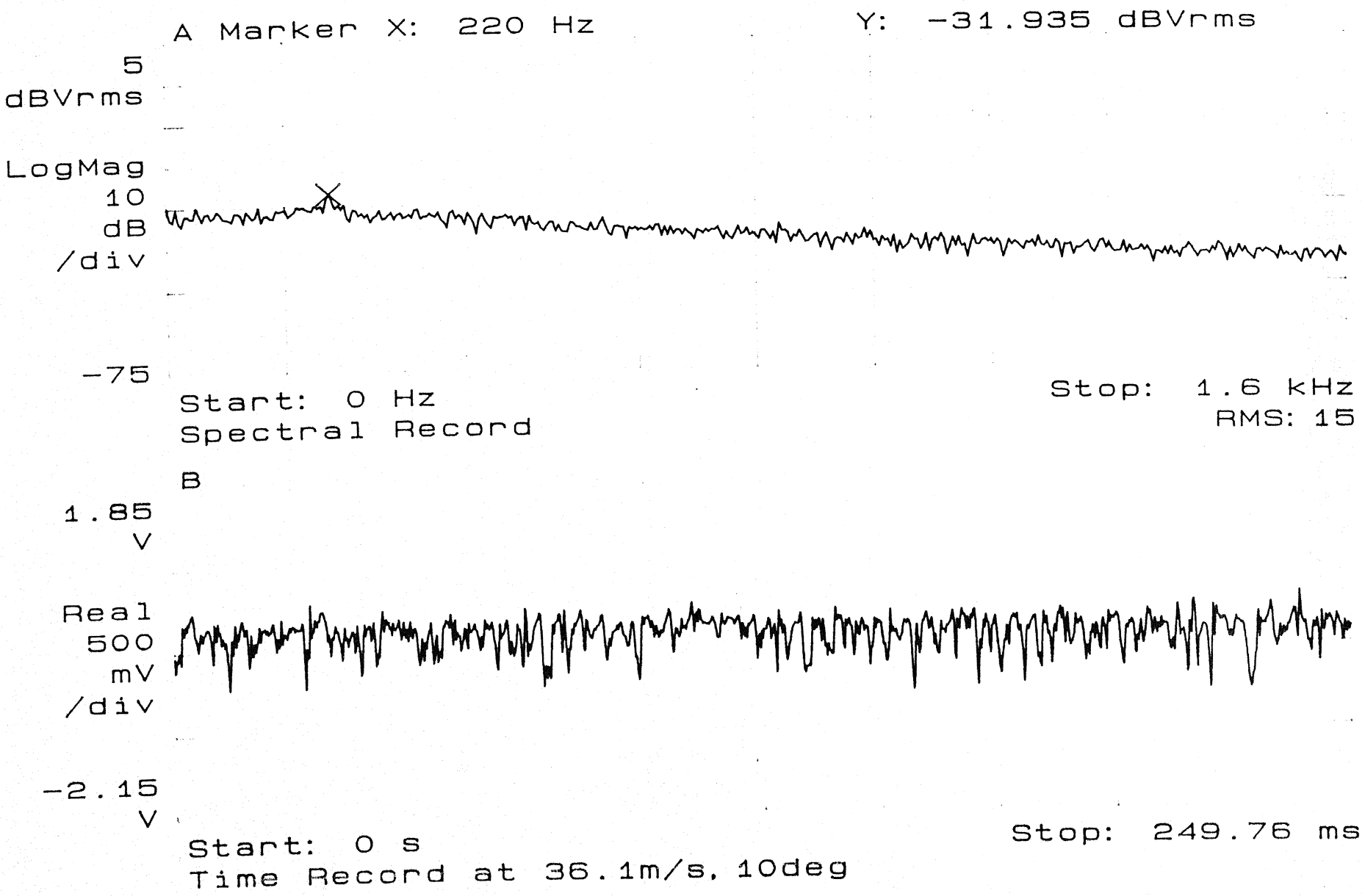
A Marker X: 220 Hz
Y: -31.935 dBVrms
5
dBVrms
LogMag
10
dB
/div
-75
Start: 0 Hz
Spectral Record
Stop: 1.6 kHz
RMS: 15
B
1.85
V
Real
500
mV
/div
-2.15
V
Start: 0 s
Time Record at 36.1m/s, 10deg
Stop: 249.76 ms

AE-1991-M-BHA-AER